

**CARBON BURIAL IN SOILS OF THE GREAT MARSH, DE:
EVALUATING ACCUMULATION RATES
AND ORGANIC MATTER COMPOSITION**

by

Rachel Jade Owrutsky

A thesis submitted to the Faculty of the University of Delaware in partial fulfillment of the requirements for the degree of Master of Science in Marine Studies

Fall 2022

© 2022 Rachel Jade Owrutsky
All Rights Reserved

**CARBON BURIAL IN SOILS OF THE GREAT MARSH, DE:
EVALUATING ACCUMULATION RATES
AND ORGANIC MATTER COMPOSITION**

by

Approved: _____
Andrew Wozniak, Ph.D.
Professor in charge of thesis on behalf of the Advisory Committee

Approved: _____
Katharina Billups, Ph.D.
Chair of the School of Marine Science and Policy

Approved: _____
Fabrice Veron, Ph.D.
Dean of the College of Earth, Ocean, and Environment

Approved: _____
Louis F. Rossi, Ph.D.
Vice Provost for Graduate and Professional Education and
Dean of the Graduate College

ACKNOWLEDGMENTS

My experience at the University of Delaware here in Lewes has been insightful, difficult, exciting, challenging, way too virtual, and empowering. I wouldn't have been able to graduate without all of my amazing support systems. This thesis is a testament to my accomplishments here and proof that I survived graduate school in a pandemic.

Andrew, thank you for taking me in at the last minute, believing in me, challenging me, encouraging me, leading me through the chaos that is academia, being understanding and patient, and letting me make decisions that I know are best for me. I've learned so much from you and I can only hope to have a mentor as considerate, insightful, and inclusive as you in the future. Thank you, Suni and George, for supporting me academically on this journey. I couldn't have done any of this work without the generous donation of George's lab space for me to cut up dirt and extract stinky porewater. I'd also like to thank the American Chemical Society Petroleum Research Fund. This work would not have been possible without its investment in this research and my academic goals. Thanks to my SMSP Student Travel Award, I was able to attend the 2022 Ocean Sciences Meeting, a rather large conference where I was able to present my work to a broader audience of researchers.

Thank you, Alina, for your commitment to the students in the Wozniak lab. Not only did you help me section cores, extract (your favorite) eggy porewater, and give me tips on a plethora of other techniques, you kept me company and gabbed with me, making the lab an even more comfortable place to work every day. The WozMOG

group is very lucky to have you. Abby, thank you for not only being a great mentee last summer, but for being a great friend. Your appreciation of DQ and pipettes inspires me to be more grateful for the little things in life.

Thank you, Neil, for not only guiding me through the intricacies of radionuclide geochemistry but also for giving me an opportunity to explore my initial interest of geochemistry back when I was an undergrad at UD. Alex Goranov, Jerry Poirier, Mahmoud Sherif, Linnea Heraty, and Christian Schwarz: you all supported me in different ways throughout my master's work and I thank you for that.

Connor, I love you so much and I cannot thank you enough for your endless support throughout my master's and everything in between these last two years. From home-cooked meals and grocery shopping to reassuring pep talks and PT-quality foot rubs, your efforts do not go unnoticed - they mean the world to me. Mom, thank you for picking up whenever I call - whether you're in another country or I'm actively playing frisbee. Your patient guidance quickly steadies me in moments of confusion or doubt. Dad and Zoe, you both have been there for me when I needed you and I thank you for that. I love you all very much. Jay, Kathy, Sara, Kieran, Lexi, and Jordan, my second family, I love you all and I am so grateful for your support (and for that pool!). Special thanks to Jay and Kathy for putting us up for the first few months that we were down here. Suz, Britt, and Leah, you keep me laughing through it all. Your love and support mean the world to me. Balegne. Last but certainly not least, I got by with a little help from my friends down in Lewes, especially Jen, Jess, Malique, Yang, and Steph. Cheers to a UD career of 6 frickin' years. Go blue hens. Bacock!!

TABLE OF CONTENTS

LIST OF TABLES	vii
LIST OF FIGURES	viii
ABSTRACT	xi

Chapter

1	CARBON ACCUMULATION AND ORGANIC MATTER COMPOSITION IN SOILS OF THE GREAT MARSH, DE.....	1
1.1	Introduction	1
1.2	Methods	6
1.2.1	Site Description	6
1.2.2	Sample Collection	7
1.2.3	Sample Processing and Storage.....	10
1.2.3.1	Extraction of Humic Acid	11
1.2.4	Porewater Analysis	12
1.2.4.1	Iron(II) and sulfide	12
1.2.4.2	Dissolved Organic Carbon	13
1.2.4.3	Fluorescent and Chromophoric Dissolved Organic Matter (FDOM)	14
1.2.5	Bulk Soil and Humic Acid Analyses.....	15
1.2.5.1	Organic carbon, total nitrogen, hydrogen, and sulfur quantification	15
1.2.5.2	Radionuclide profiles in soil cores	16
1.2.5.3	Accumulation Rate Calculations	17
1.2.5.4	Characterization by Solid State Multiple Cross- Polarization Magic Angle Spinning ¹³ C Nuclear Magnetic Resonance (multi-CP MAS ¹³ C NMR)	18
1.3	Results and Discussion	19
1.3.1	Soil OC Depth Profiles	19
1.3.2	Mass and Carbon Accumulation	22
1.3.3	Composition of OM Pools.....	34
1.3.3.1	¹³ C NMR.....	34

1.3.3.2	Porewater DOC and EEMs.....	47
1.3.3.3	Sulfurized OM	50
1.4	Concluding Remarks and Suggestions for Future Work.....	55
REFERENCES	61
Appendix		
FIGURES	72
TABLES	78

LIST OF TABLES

Table 1.1:	Core identification and descriptions.....	8
Table 1.2:	Mass accumulation and OC accumulation rates of all 4 cores integrated over the entire length of the ^{210}Pb -dated core.....	22
Table 1.3:	OC accumulation rates of all 4 cores integrated over varying timescales. 57 and 58-year timescales were obtained using ^{137}Cs . 31.2 ± 1.4 , 59.1 ± 2.6 , 92.6 ± 6.0 and 144 \pm 15-year timescales were obtained using ^{210}Pb . ^{210}Pb -based accumulation rates are reported as yearly weighted averages.	30
Table 1.4:	Relative standard deviations of the OC accumulation rates of all 4 cores over different ^{210}Pb -based timescales.	31
Table 1.5:	Comparison of OC accumulation rates of this study to regional and global rates.	32
Table 1.6:	Chemical shift assignments for integrated regions observed in ^{13}C NMR data.	35
Table 1.7:	Chemical shift assignments for peaks observed in ^{13}C NMR data.....	36
Table A1:	Depth intervals used to calculate varying accumulation rates throughout cores. Listed in terms of mass depth, OC mass depth, and length of time.....	78
Table A2:	Soil section depths and corresponding ^{210}Pb - and ^{137}Cs -dated soil ages.....	79
Table A3:	HS^- porewater concentrations in cores collected in October 2020 and June 2021.....	81
Table A4:	Fe^{2+} porewater concentrations in cores collected in October 2020 and June 2021.....	84

LIST OF FIGURES

Figure 1.1: Sampling location in the Great Marsh, DE.	7
Figure 1.2: <i>Spartina alterniflora</i> phenophases in Delaware, USA. Adapted from Vásquez-Lule and Vargas (2021).	9
Figure 1.3: Soil compaction caused by push and hammer coring.	10
Figure 1.4: Soil OC depth profiles of cores collected in October and June in vegetated and unvegetated marsh areas. The top two and bottom two figures show the same four profiles (V1, UV1, V2, and UV2), but are separated to highlight vegetative (top) and seasonal (bottom) differences. Dashed lines indicate the bottom of the root zone in V1 (34.5 cm) and V2 (27.3 cm).	21
Figure 1.5: Unsupported ^{210}Pb activity vs. mass depth. Dashed lines indicate the bottom of the root zone in V1 (6.39 g cm^{-2}) and V2 (7.65 g cm^{-2}). Colors represent time periods of different mass accumulation rates. The line of best fit equation and R^2 value are listed and color-coded. Letters A, B, and C correspond to mass accumulation rates listed in Table 1.2.	23
Figure 1.6: Unsupported ^{210}Pb activity vs. OC mass depth. Dashed lines indicate the bottom of the root zone in V1 (0.85 g cm^{-2}) and V2 (0.86 g cm^{-2}). Colors represent time periods of different OC accumulation rates. The line of best fit equation and R^2 value are listed and color-coded. Letters A, B, and C correspond to OC accumulation rates listed in Table 1.2.	24
Figure 1.7: OC accumulation rates over varying timescales calculated using ^{210}Pb -dated soils. October vegetated (maroon) and unvegetated (gray), June vegetated (green) and unvegetated (blue) cores are separated to highlight differences within each core.	28
Figure 1.8: ^{13}C NMR signals of bulk soils from the surface/root, remineralization, and burial zones from all cores collected in October 2020 and June 2021. The peak labels correspond to chemical shift assignments described in Table 1.7.	37
Figure 1.9: ^{13}C NMR signals of humic acid from the surface/root, remineralization, and burial zones from all cores collected in October 2020 and June 2021. The peak labels correspond to chemical shift assignments described in Table 1.7.	39

Figure 1.10: Relative abundances of functional groups detected in ^{13}C NMR spectra and integrated for regions defined in Table 1.6. The core ID is denoted in the upper left corner of each bar plot. Within each core, data from bulk soil and HA surface, mid-depth, and deep sections are displayed.....	42
Figure 1.11: Relative abundances of functional groups detected by ^{13}C NMR signals and integrated by regions defined in Table 1.6. The surface (top) and burial (bottom) zones of bulk soil and HA from all cores are compared to show increasing compositional homogeneity with depth...	46
Figure 1.12: Porewater DOC depth profiles of October (left) and June (right) cores. Dashed lines indicate the bottom of the root zone in V1 (34.5 cm) and V2 (27.3 cm).....	48
Figure 1.13: Soil OC and porewater HIX depth profiles taken from cores in October 2020 (left) and June 2021 (right). Dashed lines indicate the bottom of the root zone in V1 (34.5 cm) and V2 (27.3 cm).....	49
Figure 1.14: Correlations between soil OC and porewater HIX.....	50
Figure 1.15: Humic acid C/S depth profile of cores collected in October 2020 and June 2021. Dashed lines indicate the bottom of the root zone in V1 (34.5 cm) and V2 (27.3 cm). *The V1 surface value (1.5 cm) was 538.2 mol/mol.	52
Figure 1.16: HS^- porewater concentrations over depth in cores collected in October 2020 and June 2021. Dashed lines indicate the bottom of the root zone in V1 (34.5 cm) and V2 (27.3 cm). Note that V1 and UV1 profiles have different x-axes than V2 and UV2 profiles.....	54
Figure 1.17: Fe^{2+} porewater concentrations over depth in cores collected in October 2020 and June 2021. Dashed lines indicate the bottom of the root zone in V1 (34.5 cm) and V2 (27.3 cm).	55
Figure A1: Soil TN depth profiles of vegetated (left) and unvegetated (right) cores to highlight vegetative (top) and seasonal (bottom) differences. Dashed lines indicate the bottom of the root zone in V1 (34.5 cm) and V2 (27.3 cm).....	72
Figure A2: Correlation between soil TN and porewater HIX.....	73

Figure A3: Humic acid C/bulk soil OC depth profile of cores taken in October 2020 and June 2021. Dashed lines indicate the bottom of the root zone in V1 (34.5 cm) and V2 (27.3 cm). 74

Figure A4: Humic acid C/N depth profile of cores taken in October 2020 and June 2021. Dashed lines indicate the bottom of the root zone in V1 (34.5 cm) and V2 (27.3 cm). 75

Figure A5: Soil S (organic + pyrite S) depth profiles of cores collected in October and June in vegetated and unvegetated marsh areas. Dashed lines indicate the bottom of the root zone in V1 (34.5 cm) and V2 (27.3 cm). 76

Figure A6: Humic S depth profiles of cores collected in October and June in vegetated and unvegetated marsh areas. Dashed lines indicate the bottom of the root zone in V1 (34.5 cm) and V2 (27.3 cm). 77

ABSTRACT

Salt marshes have been reported to bury organic carbon (OC) up to 50x faster than temperate terrestrial forests ($244.7 \pm 26.1 \text{ g m}^{-2} \text{ yr}^{-1}$, $5.1 \pm 1.0 \text{ g m}^{-2} \text{ yr}^{-1}$). Estimates vary widely ($18\text{-}1713 \text{ g C m}^{-2} \text{ yr}^{-1}$) though, and studies that estimate OC accumulation rates for terrestrial forests use much longer timescales (70-15,000 years) than those reported for salt marshes (<150 years). Furthermore, the physical and biogeochemical controls on C storage in salt marsh soils are not fully understood, and there is a need for studies that relate organic matter (OM) composition to C storage estimates. In this study, OC accumulation rates were calculated using both ^{137}Cs and ^{210}Pb dating for four salt marsh soil cores collected in October 2020 and June 2021 in the Great Marsh, DE. ^{210}Pb -derived (144 ± 15 years) and ^{137}Cs -derived (57.5 ± 0.5 years) dating methods produced OC accumulation rates of $65.7 \pm 13.3 \text{ g C m}^{-2} \text{ yr}^{-1}$ and $144 \pm 22 \text{ g C m}^{-2} \text{ yr}^{-1}$, respectively. OC accumulation rates were additionally shown to be more variable when calculated over shorter, ^{137}Cs -based timescales. C accumulation rates calculated over short timescales (<60 years) are inflated due to a greater contribution of labile, seasonally cycling OC in the root zone. The relative standard deviation of OC accumulation rates between the four cores decreased as timescale increased, indicating increased accuracy of estimates with increasing timescale. OC accumulation rates reported in scientific literature are only comparable when using the same or similar timescales. Only the ^{137}Cs -based C accumulation estimate from this study was comparable to regionally (NW Atlantic $134.0 \pm 12.8 \text{ g m}^{-2} \text{ yr}^{-1}$) and globally ($244.7 \pm 26.1 \text{ g m}^{-2} \text{ yr}^{-1}$) reported rates, likely because most studies use ^{137}Cs or marker horizons to estimate blue C burial rates rather than ^{210}Pb or ^{14}C that date soils over longer timescales ($^{210}\text{Pb} \leq 200$ years; $^{14}\text{C} \leq 60,000$ years). The blue

C community may thus be currently reporting inflated OC burial rates. These rates need to be recontextualized within their associated timescales. In addition to timescale, depth is also of major importance when calculating C accumulation rates. A balance of any seasonal, labile OC inputs with remineralization-induced outputs is necessary to attain an accurate C accumulation rate, independent of vegetative or seasonal influence. Based on the soil OC profiles from this study and a handful of other published works, I suggest collecting cores of at least 50 cm in order to achieve this balance. However, if the research question at hand requires the use of shorter timescales, this recommendation would become irrelevant.

The organic matter (OM) composition at selected depth ranges was also characterized to evaluate the forms of OC that accumulate over time to better understand the forms of C being stored in marsh soils. Soil and humic acid (HA) molecular properties were characterized at discrete depths via elemental analysis, ^{13}C NMR, UV/Vis and EEMs spectroscopy. Overall, the variability in soil and humic acid characteristics decreased with depth, suggesting increasing homogeneity in salt marsh soil OM properties over the course of burial and early diagenetic processes below the root zone. Soil OC concentrations were highly variable at the surface but decreased and converged to similar values at depth. Similarly, HA C/S ratios were high at the surface but decreased and converged over depth, potentially indicating sulfurization and selective retention of organic sulfur compounds. HAs from all four cores showed increasing structural similarity over depth with marsh aromatic C contributions increasing with core depth. The increasing structural similarity with depth suggests that apparent vegetative, seasonal, and possibly tidal influences on HA properties observed at the surface dissipate during early diagenesis. Future molecular level

characterization is needed to evaluate whether certain compounds or compound classes (i.e., sulfurization products) may be selectively preserved and/or which potential mechanisms (e.g., selective preservation, mineral interactions, dilution, environmental conditions) are most important for burying C in salt marsh soils.

Chapter 1

CARBON ACCUMULATION AND ORGANIC MATTER COMPOSITION IN SOILS OF THE GREAT MARSH, DE

1.1 Introduction

Humans have been burning carbon (C) in the form of fossil fuels for the last ~150 years, setting atmospheric CO₂ levels higher than they've been in the last one million years (Petit et al., 1999), spurring anthropogenically induced climate change. Environments on Earth act as buffers and, through photosynthesis, convert this inorganic carbon into organic carbon (OC). This OC, the major component within organic matter (OM), either gets remineralized back to CO₂ through biotic or abiotic processes or is sequestered in terrestrial, estuarine, or marine sediments, effectively removing CO₂ from the atmosphere on climate change-relevant timescales.

Historically, natural C sequestration research has focused on either ocean or terrestrial forest ecosystems. Within the last 20 years however, a new category of ecosystems has been recognized as a key contributor to atmospheric CO₂ removal (or OM preservation): vegetated coastal ecosystems including mangroves, seagrasses, and salt marshes which are collectively known as blue carbon environments (Nellemann et al., 2009). Being some of the most productive ecosystems on the planet (Schelske and Odum, 1962) in combination with their relatively high organic inputs, sedimentation rates and resultant anoxic sediments, blue carbon environments are equipped to store large amounts of C.

Numerous studies have quantified salt marsh C burial (interchangeably used with “accumulation”) rates (St. Laurent et al., 2020; Van de Broek et al., 2016; Loomis and Craft, 2010; Unger et al., 2016; Kelleway et al., 2017; Yuknis, 2012; Duarte et al., 2005) which collectively suggest salt marshes to bury OC (244.7 ± 26.1 g C m⁻² y⁻¹; Ouyang and Lee, 2014) up to 50 times faster than temperate terrestrial forest environments (5.1 ± 1.0 g C m⁻² y⁻¹; McLeod et al., 2011; Chmura, 2013). Although salt marshes cover a much smaller surface area worldwide ($2.2\text{-}40 \times 10^4$ km²; Chmura et al., 2003; Duarte et al., 2005) than temperate forests (1.04×10^7 km²; Schlesinger and Bernhardt, 1997), these high burial rates make their global carbon burial rates comparable to terrestrial and oceanic systems (salt marshes 5-87 Tg C y⁻¹, temperate forests 53 Tg C y⁻¹, oceans 243 Tg C y⁻¹; Chmura et al., 2003; Duarte et al., 2005; Schlesinger and Bernhardt, 1997; Zehetner, 2010; Nellemann et al., 2009). Thus, current data show that salt marshes account for C storage services disproportional to their global surface area, rendering them equally or more important to our understanding of OM preservation, and in turn, the global carbon cycle. However, the range of salt marsh C burial estimates is large (18-1713 g C m⁻² y⁻¹; McLeod et al., 2011) and can potentially be explained by differences in sampling procedures and environmental conditions (Morris and Callaway, 2018; Bianchi et al., 2018). Much work is needed, therefore, to understand the factors that influence the wide range of variability in C storage estimates.

The methodology and timing of core collection are known to impact C accumulation rates in marsh soils. Most salt marsh C burial studies utilize the shallow core approach (Ouyang and Lee, 2014) because shallow cores are easier and cheaper to extrude than long cores. Surface soils (<30 cm) contain a higher percent of labile C

than deeper soils (Morris and Callaway, 2018). Studies that use shallower cores integrate C burial over inherently shorter, decadal timescales and, as a result, produce inflated accumulation rates relative to studies that integrate over longer, centennial timescales. This phenomenon is widely recognized in the field of geology as the “Sadler effect” (Sadler, 1999). In soil sciences, studies use timescales of 700-15,000 years to report OC burial rates (Zehetner, 2010), including the rate reported above ($5.1 \pm 1.0 \text{ g C m}^{-2} \text{ y}^{-1}$; McLeod et al., 2011). Zehetner (2010) showed that burial rates decrease exponentially with increasing timescales. This phenomenon has been discussed in just a handful of studies in the blue C field (Tucker, 2016; Champlin et al., 2020; Morris and Callaway, 2018; DeLaune et al., 2018; Holmquist et al., 2018; Holmquist et al., 2021). Some blue C studies do use longer cores to calculate OC accumulation rates which could explain the large range of estimates ($18\text{-}1713 \text{ g C m}^{-2} \text{ y}^{-1}$; McLeod et al., 2011), but the mean reported OC burial rates in salt marshes are biased toward studies that use shorter cores and report relatively higher C accumulation rates.

Broadly speaking, salt marsh OC accumulation rates can vary geographically depending on both anthropogenic and natural factors such as local sea level rise, tidal amplitude, and latitude (Bianchi et al., 2018; Ouyang and Lee, 2014), factors that ultimately affect the sedimentation rate (Nyman et al., 2006). Sedimentation is the accretion of both inorganic and organic materials and is locally influenced by proximity to the tidal creek (Friedrichs and Perry, 2021), maximum primary productivity, salinity (related to above-ground vegetation growth; Van de Broek et al., 2016), and below-ground vegetation growth. Vegetation on the surface of a salt marsh slows the rate of the incoming tides and traps sediments, increasing the sedimentation

rate of the marsh in that location (Stumpf, 1983). Therefore, the presence of above-ground vegetation may impact OC inputs as well as the physical burial of OC via sedimentation.

Seasonality may also impact the reported OC accumulation values. The phenology of the dominant salt marsh grass in the Great Marsh, *Spartina alterniflora*, has been observed to control the seasonal inorganic C flux within a temperate salt marsh (Vázquez-Lule and Vargas, 2021). In Delaware during Greenup (start of growth, April to June) and Maturity (growth peak, July to September), there is net CO₂ uptake with higher uptake levels during Maturity due to increased photosynthetic activity. During Senescence (decline in and death of vegetation, September to October) and Dormancy (dormant grasses, November to March), there are net CO₂ emissions and an increase in labile OM as the vegetation decomposes. The primary CO₂ uptake and emission processes are biological in nature and likely contribute to variations in the surface soil OC inventories along with hydrologically-driven lateral transport of OC to estuaries. Any of these sources and sinks of OC to surface soils can alter soil OC inventories on seasonal timescales and yield C accumulation rates that vary with season. The extent to which these surface soil OC inventory variations affect OC burial rates at greater depths (decadal scales) is unclear.

The composition of OM may also influence OC burial rates (Morris and Callaway, 2018; Unger et al., 2016; Enríquez et al., 1993). Organic sulfur compounds, for example, have been shown to form in salt marsh soils through the process of sulfurization (Ferdelman et al., 1991) and be more resistant to degradation than their labile OM counterparts (Bianchi and Canuel, 2011; Pohlabein et al., 2017). Higher inorganic inputs have been shown to promote OM mineral association or protection

(Sun et al., 2019; Burdige, 2007), a mechanism where minerals bind to and protect OM from degradation. The intrinsic chemical properties of OM itself may also prevent degradation via an inherent microbial inaccessibility or promoting mineral associations, which in turn prevents degradation (Stevenson, 1994; Burdige, 2007).

During burial, labile and recalcitrant OC go through biotic and abiotic transformations in a sedimentary process known as diagenesis (Tissot and Welte, 1984), a millenia-long process that ultimately results in the formation of coal. During early diagenesis, labile OM is remineralized, leaving behind recalcitrant monomers that eventually condense into geopolymers called humic substances. Humic substances consist of humic acids (HAs), fulvic acids, and humin. Though the relevance of this operationally-defined pool of OM is hotly debated (Lehmann and Kleber 2015; Olk et al., 2019; Kleber and Lehmann 2019), HAs have been shown to be important in reducing the longevity of pollutants in aquatic systems (Grannas et al. 2012), reducing the mobility of pesticides and retaining plant-viable metal ions in soils (Olk et al., 2019 and references therein). In the context of blue carbon, HAs are of interest because their inherent chemical stability in soils (Stevenson, 1994) makes them an important component of the accumulating recalcitrant carbon in soils. The composition of the refractory HA pool within salt marsh soils is not well characterized. Given the potential role for molecular characteristics in contributing to C storage (i.e., via intrinsic stability or interactions with minerals), studies of marsh OM composition will help explain variations in blue C inventories and accumulation rates.

To advance our understanding of salt marsh OC burial rates and the composition of the buried OM, 2 cores were collected in the high marsh in both

October of 2020 and June of 2021. During each timepoint, one core was collected in an area populated by *S. alterniflora* and one in a bare mudflat area of the marsh. Each core was sectioned and characterized to obtain depth profiles for its OC composition and functional group abundance (via ^{13}C nuclear magnetic resonance (NMR) and excitation emission matrix spectroscopy) as well as its inorganic porewater iron and sulfide content. The data are presented here in an investigation of how *S. alterniflora* phenology, vegetation presence (or lack thereof), and timescale of interest affect (1) OC accumulation rate estimates and (2) depth profiles of labile and recalcitrant OM characteristics in the Great Marsh, Lewes, DE. The results of this work have bearing on best practices for calculating OC accumulation rates and understanding the forms of OM that are preserved over centennial timescales that will interest coastal carbon biogeochemists.

1.2 Methods

1.2.1 Site Description

The Great Marsh is a salt marsh located on the Southern coast of the Delaware Bay just Northwest of the University of Delaware's College of Earth, Ocean, and Environment Hugh R. Sharp Campus in Lewes, DE (Figure 1.1). It covers approximately 17,000 acres of land that is impacted by mosquito ditching, a common practice for east coast USA marshes that peaked in the 1930s (Daiber 1974). This marsh is dominated by semi-diurnal tides with a mean range of 1.3 m, a spring range of 1.6 m (Roman and Daiber 1989) and mainly drains into the Broadkill River. The sampling site is considered high marsh and gets inundated twice a month. *Spartina alterniflora* is the dominant salt marsh vegetation in much of the marsh including the

sampling locations. For purposes of biogeochemical comparisons, the locations of the sampling site (Figure 1.1) within the Great Marsh are similar to those used by Ferdelman et al. (1991), Luther and Church (1988), and Boulegue et al. (1982).



Figure 1.1: Sampling location in the Great Marsh, DE.

1.2.2 Sample Collection

A total of four cores (~1 m in length, 5.7 cm in diameter) were collected from the Great Marsh. Long cores were needed to capture temporal variability over decadal and centennial timescales. Two cores were collected on both October 28, 2020 and June 1, 2021: one collected from an area with aboveground vegetation and one from an area without vegetation (hereafter referred to as “vegetated” and “unvegetated,” respectively), to capture vegetation-induced changes in C accumulation and composition. October cores were collected three days before the second spring neap tide of the month while June cores were collected in between the two neap tides.

Throughout this thesis, cores will be referenced by their identifications as described below.

Table 1.1: Core identification and descriptions.

Core ID	Collection Date	Aboveground Vegetation	Total length (cm)
V1	October 28, 2020	yes	102
UV1	October 28, 2020	no	72
V2	June 1, 2021	yes	80.6
UV2	June 1, 2021	no	86.4

Cores were collected within 100 m from one another and at least 30 m inland from the tidal creek to eliminate bioturbation and cordgrass species variability. The dominant cordgrass present in this high marsh area was short-form *Spartina alterniflora*. All cores were collected 1-2 hours before low tide to reduce tidal variability.

S. alterniflora cordgrass goes through growth, or phenological, phases (phenophases) that somewhat overlap with fall, winter, spring, and summer in Delaware. The phenophases of *S. alterniflora* in Delaware are determined by a green chromatic coordinate (GCC; Brown et al., 2017; Vasquez-Lule and Vargas 2021) as observed by a PhenoCam in the St. Jones Reserve, a salt marsh located in Dover, DE, approximately 40 mi north of Lewes. Increasing and peak GCC values, associated with growing and peak growth phenophases, were deemed Greenup and Maturity,

while decreasing and minimum GCC values, associated with Senescent and Dormant phenophases, were deemed Senescence and Dormancy (Figure 1.2). Assuming grasses in the St. Jones Reserve go through these phenophases around the same time as Great Marsh grasses, the sampling dates in this study correspond to Senescence (October 28; GCC = 0.326) and Greenup (June 1; GCC = 0.376).

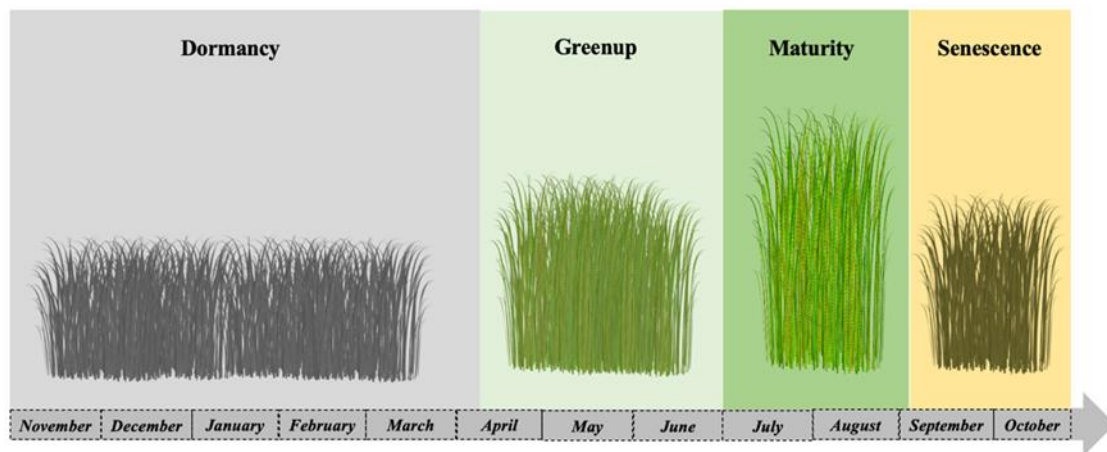


Figure 1.2: *Spartina alterniflora* phenophases in Delaware, USA. Adapted from Vásquez-Lule and Vargas (2021).

Cores were collected using the push core technique. A plexiglass coring tube was first hammered into the soil. The coring tube top was sealed and the core was removed using either a 36 in. Bulldog farm jack (October) or after digging a hole around the core and pulling the core out of the ground manually at a slight angle (June). A custom-made core cap was inserted immediately into the bottom of the core once accessible to prevent further loss of soil and maintain anoxia. The coring tube was brought back to the lab (same day) for sectioning. Core compaction due to the hammering process was calculated by measuring the distance between the top of the

coring tube and the soil on the inside and outside of the coring tube (Figure 1.3; Carr et al., 2020), as described in Equation (1). The compaction factor was applied to the entirety of the core and was used to calculate the true depth of core sections. The average of the depth interval was used to plot the data in this thesis (e.g. the top 2-cm section of a core is plotted at 1 cm).

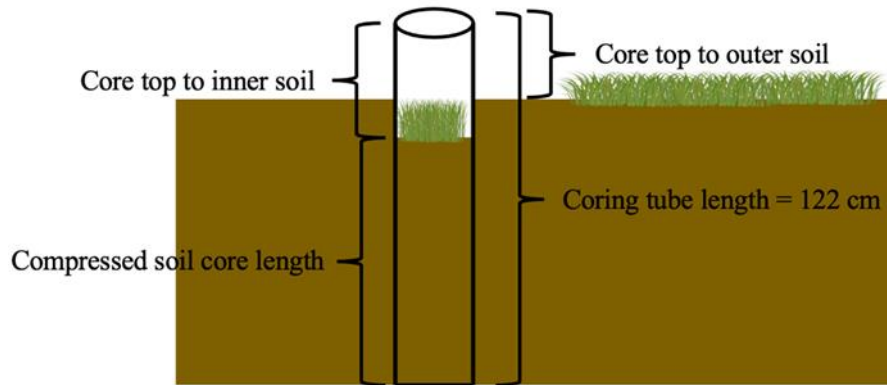


Figure 1.3: Soil compaction caused by push and hammer coring.

$$\text{Compaction factor} = \frac{\text{True core length}}{\text{Compressed core length}} = \frac{122 - \text{core top to outer soil}}{122 - \text{core top to inner soil}} \quad (1)$$

1.2.3 Sample Processing and Storage

In the lab, cores were sectioned into 2 cm sections in a glove bag filled with ultra-high purity N₂ or Ar. Each section was divided into two 50 mL centrifuge tubes and centrifuged to separate the porewater from the soil. The porewater was immediately filtered through a 0.45 μm Teflon filter into a 20 mL scintillation vial in a glove bag filled with ultra-high purity N₂ or Ar. Porewaters were stored in vials at 4°C under an inert atmosphere (ultra-high purity N₂ or Ar) until all porewater analyses were complete, no longer than two weeks after the sampling date. As noted below,

chemical species prone to oxidation were analyzed ≤ 2 days After this time, porewaters were stored frozen at -20°C . The remaining wet soils were also stored frozen at -20°C until soil analysis could begin. Prior to soil analysis, soils were dried at $55\text{-}60^{\circ}\text{C}$, sieved with a 4 mm sieve, and homogenized using a spice grinder. Homogenized soil sections were stored frozen at -20°C until sample analysis or further processing.

1.2.3.1 Extraction of Humic Acid

Humic acids were extracted following a modified version of a commonly used HA extraction technique (Lamar et al., 2014). Briefly, a 5 g dry bulk soil:200 mL 0.1 M NaOH (sonicated and degassed) ratio was used for triplicate base extraction. Sodium hydroxide extractions are unlikely to affect the chemical make-up of organic matter but will increase the relative abundance of aromatic C and decrease carbohydrate-like C (apparent in ^{13}C NMR data; Chen et al. 2019). The solution was shaken for 24 hours and subsequently centrifuged at 4000 rev/min and decanted. The precipitate (humins) was freeze-dried, capped with N_2 , and stored at -20°C . The approximately 600 mL of combined base extracts containing fulvic and humic acids were filtered using a $0.7\ \mu\text{m}$ GF/F pre-combusted filter to remove particulates. The solution was acidified to pH 1 using HCl, covered with N_2 , and shaken for 12 hours. After another 12 hours at 4°C , HA had precipitated and accumulated at the bottom of the glass bottle. The solution was centrifuged to separate fulvic acids from humic acids. HAs were freeze-dried, capped with N_2 , and stored at -20°C until sample analysis or further processing. Fulvic acids were stored at -20°C .

Six sections from each core were chosen to extract HAs. Two sections within the depths of $\sim 0\text{-}25$ (root zone, depths may vary), $\sim 25\text{-}50$ (bottom of the root zone to

50 cm), and 50-100 cm were defined based on soil OC profiles (Figure 1.4) and were used to understand OM transformations over the course of burial within early diagenesis. Specifically, these regions capture the chemical gradient from 1) the surface/root zone that contains more recently-produced and seasonally cycling soil OM (~0-25 cm) to 2) depths below the bottom of the root zone (~25-50 cm) where OC concentrations are observed to decline and which may contain a mix of semi-labile and recalcitrant soil OM to 3) depths further down (50-100 cm) where OC concentrations are observed to stabilize and which are expected to contain the highest percentage of recalcitrant OM. These three depth ranges will be referred to hereafter as the 1) surface/root zone, 2) remineralization zone, and 3) burial zone.

1.2.4 Porewater Analysis

1.2.4.1 Iron(II) and sulfide

The extracted porewater was analyzed for Fe^{2+} and HS^- concentrations via UV/Vis spectrophotometry with an HP 8452 Diode Array Spectrophotometer and a 1 cm pathlength UV cell using methods developed by Stookey (1970) and Luther et al. (2011), respectively. Because sulfides are susceptible to oxidation under oxic conditions at 25°C with a half-life of 1-2 days (Millero et al., 1987), extracted porewaters were stored in vials under inert conditions (ultra-high purity N_2 or Ar) at 4°C, increasing the half-life of the sulfides present. Regardless, measurements were completed within 48 hours of sample collection.

Sulfide species present in salt marsh porewaters (pH ~4-7.5; Luther and Church 1988) include hydrogen sulfide (H_2S) and bisulfide (HS^-). To measure HS^- ,

porewater was added to a mixture of water and 0.2 M sodium bicarbonate buffer (pH 9-9.5) in a ratio of 9:1 by volume. H_2S becomes HS^- at this pH. The sum of H_2S and HS^- were detected as HS^- at 230 nm (Ellis and Golding 1959). Standards were made by dissolving sodium sulfide nonahydrate ($\text{Na}_2\text{S}\cdot 9\text{H}_2\text{O}$, rinsed with deionized water and dried prior to weighing) in deionized water purged with ultra-high purity N_2 or Ar to make a 0.005 M solution. Calibration curves using 0 to 100 μM HS^- were used to determine unknown sample concentrations.

To measure Fe^{2+} , porewater was added to a mixture of water, 2.5 M ammonium acetate, and 0.01 M ferrozine in a ratio of 9:1:0.1 by volume. The Fe^{2+} present in the sample creates a complex with ferrozine which absorbs at 562 nm. Fe^{2+} standards were made by dissolving ferrous ammonium sulfate in deionized water purged with ultra-high purity N_2 or Ar to make a 0.005 M solution. Calibration curves using 0 to 30 μM Fe^{2+} were used to determine unknown sample concentrations.

1.2.4.2 Dissolved Organic Carbon

Porewater dissolved organic carbon (DOC) was measured using a Shimadzu TOC-V CPH Total Organic Carbon Analyzer. Samples were acidified to pH 2 using HCl prior to analysis to convert inorganic carbon to CO_2 . CO_2 was purged prior to combustion and analysis of organic carbon. Once the sample was purged of CO_2 , the remaining non-purgeable OC was converted to CO_2 via catalytic oxidation combustion at 680°C. This CO_2 was detected by a non-dispersive infrared (NDIR) sensor and quantified as DOC. The instrument was calibrated using a five-point standard curve made by serial dilutions of a potassium hydrogen phthalate standard. Consensus Reference Materials (University of Miami's Hansell Organic Biogeochemistry Laboratory, MSR, $62 \pm 1.1 \mu\text{M}$ DOC), phenylalanine (PA), and

ethylenediaminetetraacetic acid (EDTA) were run in tandem with samples to assess instrument accuracy and check for instrument drift. An average of the best three out of five injections with a maximum coefficient of variation of 2% was used to report DOC concentrations.

1.2.4.3 Fluorescent and Chromophoric Dissolved Organic Matter (FDOM)

A Horiba Aqualog was used to conduct UV/Vis and excitation-emission matrix (EEM) spectroscopy to qualitatively analyze the spectroscopic characteristics of CDOM and FDOM in porewaters, respectively. The analysis was performed over an excitation range of 230-700 nm in 2 nm increments and an emission range of 245-822 nm in 4.7 nm increments with a UV cell of 1 cm pathlength. Peaks within EEMs indicate humic-, protein-, pigment-, tyrosine-, or tryptophan-like properties (Coble, 2007) and their relative abundances provide information on the OM origin (i.e., terrestrial, autochthonous, microbial). A manufacturer's excitation check and emission check were performed prior to each analysis. Data were processed by the software and were standardized using an average of 5 scans of Raman scattering. The staRdom R package was used to remove Rayleigh scattering, interpolate and smooth the data, and quantify well-established peak responses and the humification index (HIX). This index is proportional to relative complexity and aromaticity or humification as described by Ohno (2002) and Zsolnay (1999). HIX was calculated using Equation (2). It describes the ratio of the summed emission between 435 and 480 nm to the summed emission between 300 nm and 345 nm, both at a fixed excitation wavelength of 254 nm.

$$HIX = \frac{\sum_{em=435}^{480} X_{254,ex}}{\sum_{em=300}^{345} X_{254,ex}} \quad (2)$$

In general, once natural water samples are collected, FDOM and CDOM stability are susceptible to photochemical and microbial degradation. Therefore, it is recommended that samples be analyzed as soon as possible after collection (Spencer and Coble, 2014). Samples in this study were analyzed 8-9 days after collection. Studies show that in samples with 10-60 mg/L DOC (the range of porewater concentrations in this study), fulvic and protein-like fluorophores are reduced by less than 5% in fluorescence intensity after 10 days in storage at 4°C (Spencer and Coble, 2014). A separate experiment would be necessary to determine more precise site-specific effects of the storage conditions on these samples. Because all samples were stored in the same conditions and for the same length of time in this study, their CDOM and FDOM properties may be expected to have been affected similarly.

1.2.5 Bulk Soil and Humic Acid Analyses

1.2.5.1 Organic carbon, total nitrogen, hydrogen, and sulfur quantification

CHNS elemental analysis (EA) was performed on the bulk soil and humic acids to quantify C, N, and S. To prepare the bulk soil for analysis, 20 mg of soil was weighed into a stack of two solvent-rinsed (DCM and acetone) and dried tin capsules. Two drops of 12 M HCl were added which resulted in some deterioration of the tins. The acidified sample was dried overnight in a desiccator. A third solvent-rinsed and dried tin was used to encase the somewhat deteriorating tins and acidified sample to prevent sample loss. Acidification of the sample results in the loss of inorganic C from the C pool and acid volatile sulfur (AVS, comprised of FeS and H₂S) from the inorganic S pool as well as conversion of organic polysulfides to elemental S (Yücel et al., 2010). As a result, organic C, total N, and the sum of pyrite (FeS₂), elemental S

(S₈), humic and fulvic S, and organic polysulfides (in the form of S₈) were quantified here. Samples were analyzed alongside sulfanilamide standards using an Elementar Vario EL cube at the University of Delaware Advanced Materials Characterization Laboratory. Samples were combusted at temperatures up to 1200°C under O₂ with a flow rate of 35-38 mL/min. The N, C, S, and H were detected as N₂, CO₂, SO₂, and H₂O in that order through gas-specific adsorption columns.

Because the final step in the HA extraction involves acidifying the sample to pH 1 (see 1.2.3.1), HAs were not acidified prior to EA. 20 mg of HA were weighed into solvent-rinsed and dried tins and sent to the University of Delaware Environmental Isotope Science Laboratory to quantify humic C, humic N, and humic S. Carrier flow was 180 mL/min with helium saver enabled. The TCD reference flow was 50 mL/min. A single furnace quartz combustion tube packed with tungstic oxide and electrolytic copper was used at 1000°C. The EA was fitted with a MAS200R autosampler. The C, N, and S were quantified by a TCD signal. Data were processed using ISODAT software and Microsoft Excel. Peak areas were calibrated using a sulfanilamide standard from Elemental Microanalysis.

1.2.5.2 Radionuclide profiles in soil cores

Radionuclide profiles of ²¹⁰Pb and ¹³⁷Cs in soil cores were measured at the University of Delaware Environmental Isotope Science Laboratory. The profile of unsupported ²¹⁰Pb (from atmospheric deposition) can be used to date soils and sediments because ²¹⁰Pb activity decays continuously as sediments are being deposited. The unsupported ²¹⁰Pb in a given core section is determined by subtracting the total ²¹⁰Pb from the supported ²¹⁰Pb generated by in situ decay of ²²⁶Ra. ²¹⁰Pb has a half-life of 22.3 years and its application as a dating tool is limited to within the last

100-200 years (Yuknis, 2012). ^{137}Cs has been used to determine average sediment accretion and accumulation rates since it adsorbs to the particulate phase, and its nuclear fallout peak which can be traced to a date of 1963 decreases with time and can show up clearly in soil records. ^{137}Cs is limited as a dating tool to up to 59 years (as of 2022). ^{210}Pb (46.5 keV) and ^{137}Cs (661.6 keV) were measured by high-purity Ge gamma spectrometers (Model GWL-170-15-LB-AWT with 15-mm well diameters, EG&G Ortec, Ametek, Inc.). Spectrometers were calibrated using CanMet and NIST reference materials (see Corcoran et al., 2018 for more details). Activities were reported in becquerels per kilogram dry mass (Bq/kg). A constant rate of supply model was used to calculate sediment mass accumulation rates from sediment core profiles of unsupported ^{210}Pb activities and dry bulk densities. This model assumes the atmospheric flux of unsupported ^{210}Pb is constant when averaged over 100-200 years which allows for varying sedimentation rates (Corcoran et al., 2018; Yuknis, 2012). These two dating tools (^{210}Pb and ^{137}Cs) were cross-referenced.

1.2.5.3 Accumulation Rate Calculations

A mass accumulation rate (also known as “sediment accumulation rate”) is a measure of the mass of inorganic plus organic matter that is added to a marsh in units of $\text{g m}^{-2} \text{y}^{-1}$. Soil dates, t , and accumulation rates, r , were calculated following DeFranco et al. (2020) as follows

$$t = \frac{\ln\left(\frac{A_0}{A_Z}\right)}{\lambda} \quad (3)$$

$$r_{\text{accumulation}} = \lambda M / 0.0001 \quad (4)$$

where t is the soil age, A_0 is the cumulative excess of ^{210}Pb in the entire core (Bq cm^{-2}), A_Z is the sum of unsupported ^{210}Pb activity below depth Z (Bq cm^{-2}), λ is the decay

constant of ^{210}Pb (0.03108 yr^{-1}), r is the mass accumulation rate ($\text{g m}^{-2} \text{ y}^{-1}$), and M is the slope of the plot of $\ln(A_0/A_z)$ vs. mass depth (g cm^{-2}).

A carbon accumulation rate is a measure of the annual area-normalized carbon mass integrated over a specific time period that is added to a marsh ($\text{g C m}^{-2} \text{ y}^{-1}$). This is the term used to describe the burial or accumulation of both allochthonous and autochthonous OC in salt marsh blue C studies. To obtain the OC accumulation rate using ^{210}Pb -dated soils, the dry bulk density of each sample was multiplied by the soil %OC (quantified by EA) to get the OC mass depth. The slope of the plot $\ln(A_0/A_z)$ vs. OC mass depth (in g OC cm^{-2}) was then used in Equation 4 to get the OC accumulation rate. Calculating the OC accumulation rate using ^{137}Cs -dated soils requires a different equation, listed below (Tucker, 2016).

$$r_{OC \text{ accumulation}, 137\text{Cs}} = \frac{\sum_{i=0}^{1963 \text{ depth}} (OC_i * \rho_{di} * x_i * 10,000)}{t} \quad (5)$$

In this equation, OC_i represents the OC soil concentration (quantified by EA, in g OC/g dry soil) for the i^{th} depth interval, ρ_{di} is the soil dry bulk density (g cm^{-3}), x_i is the interval of the section (cm), and t is the difference in years between 1963 and the date of core collection.

1.2.5.4 Characterization by Solid State Multiple Cross-Polarization Magic Angle Spinning ^{13}C Nuclear Magnetic Resonance (multi-CP MAS ^{13}C NMR)

Bulk soil and HA samples were sent to the NMR Laboratory at the University of Delaware for solid state multi-CP MAS ^{13}C NMR analysis. Of the six HA samples extracted from each core, three samples were chosen for ^{13}C NMR analysis, one from each depth zone (surface/root zone, remineralization zone, and burial zone as defined in 1.2.3.1) to capture structural variability over the course of burial/early diagenesis.

These zones are defined based on the soil OC depth profiles as described in the Results and Discussion. Corresponding bulk soils from the same depths were analyzed as well. All ^{13}C NMR spectra were acquired using multiple cross polarization (multiCP) on a 600 MHz Bruker AVIII NMR spectrometer with a 3.2 mm E-Free HCN probe at a magic angle spinning (MAS) rate of 14 kHz (Johnson and Schmidt-Rohr, 2014). 16384 scans were averaged for each sample. The pulse sequence utilized eleven 0.5 ms CP periods (due to relatively short ^1H $T_{1\rho}$ values) with a delay of 0.4 s between CP periods, followed by a ^{13}C Hahn echo. Each CP period had a 90-100% ramp on ^1H . 74 kHz ^1H decoupling was applied during the Hahn echo as well as acquisition. 90° pulse lengths were 3.4 μs and 3.2 μs for ^1H and ^{13}C , respectively. Data were processed using Mestrelab Research Mnova software. NMR signals were phase-corrected and baseline-corrected with an apodization of 200 Hz.

1.3 Results and Discussion

1.3.1 Soil OC Depth Profiles

Soil OC concentrations in all four cores were highest in the top 10 cm of the soil and declined by a factor of 2-3 with depth (Figure 1.4). For comparison and consistency purposes, I define the “surface soils” in UV1/V1 and UV2/V2 core pairs as the portion of the core above where root mass was observed in the vegetated cores. For V1 and V2 the root zone extended to 34.5 and 27.3 cm, respectively. The remineralization zone was then 34.5-50 cm and 27.3-50 cm in V1/UV1 and V2/UV2, respectively, regions of the depth profile where OC concentrations were observed to decline. Finally, the region between 50-100 cm is defined the burial zone in all cores due to this depth range showing relatively constant OC concentrations. Surface OC

mass concentrations were higher by almost a factor of 2 in vegetated (V1 7.7 ± 1.5 mmol OC/g dry wt, V2 7.3 ± 1.0 mmol OC/g dry wt) relative to unvegetated cores (UV1 4.8 ± 0.9 mmol OC/g dry wt, UV2 5.3 ± 2.1 mmol OC/g dry wt.) with the OC inventories particularly diverging toward the bottom of the root zone. In V1 and V2, OC values declined by a factor of 2-3 with depth below the root zone where there are no new inputs from belowground biomass and microbial remineralization and/or lateral transport of OC removal processes dominate OC cycling. OC values were higher at the surface and declined with depth by a factor of 2-3 in UV1 and UV2 as well. Although these cores were unvegetated, the trend over depth in soil OC resembled that of the vegetated cores (i.e., OC was highest at the surface and decreased with depth). These high surface values could be due to lateral exchange from adjacent vegetated regions or OC tidal inputs or to primary production from microphytobenthos. Below 24 cm in UV1 and 12 cm in UV2, soil OC concentrations declined, suggesting that these allochthonous inputs became less influential over depth. In the burial zone, OC concentrations in all but UV2 converged to 2-4 mmol OC/g dry wt. A similar trend was observed for soil total nitrogen (TN) profiles (Figure A1). Values were high in the surface/root zone, decreased in the remineralization zone, and converged to 0.2-0.4 mmol TN/g dry wt in the burial zone.

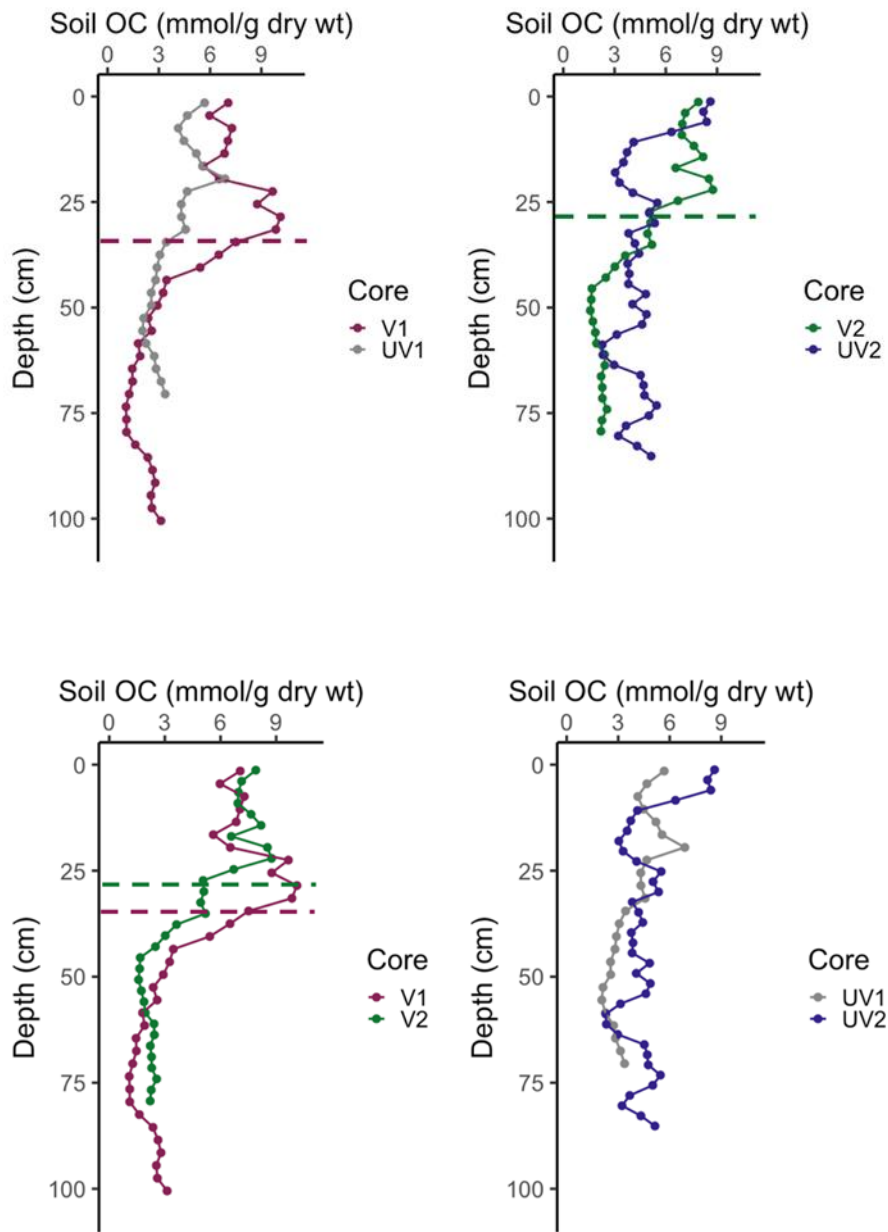


Figure 1.4: Soil OC depth profiles of cores collected in October and June in vegetated and unvegetated marsh areas. The top two and bottom two figures show the same four profiles (V1, UV1, V2, and UV2), but are separated to highlight vegetative (top) and seasonal (bottom) differences. Dashed lines indicate the bottom of the root zone in V1 (34.5 cm) and V2 (27.3 cm).

1.3.2 Mass and Carbon Accumulation

Mass accumulation and OC accumulation rates are listed in Table 1.2. ^{210}Pb activity vs. mass depth and OC mass depth are shown in Figure 1.5 and Figure 1.6, the slopes of which were used to calculate OC accumulation rates (Equation 4).

Table 1.2: Mass accumulation and OC accumulation rates of all 4 cores integrated over the entire length of the ^{210}Pb -dated core.

Core	Timescale (yr)	Mass Accumulation Rate ($\text{g m}^{-2} \text{yr}^{-1}$) ¹	OC Accumulation Rate ($\text{g m}^{-2} \text{yr}^{-1}$) ¹
V1	157	900 ± 34.8	75.7 ± 4.1 (A) 132 ± 5.2 (B) 21.7 ± 3.0
UV1	141	637 ± 12.7	48.1 ± 2.2
V2	156	584 ± 20.6 (A) 851 ± 30.2 (B) 335 ± 11.6	63.0 ± 2.3 (A) 103 ± 3.5 (B) 26.2 ± 1.2
UV2	125.4	1091 ± 83.2 (A) 520 ± 22.9 (B) 4757 ± 209 (C) 889 ± 85.4	76.2 ± 7.8 (A) 140 ± 13.3 (B) 313 ± 12.5 (C) 40.6 ± 5.3

¹Mass and OC accumulation rates were calculated using ^{210}Pb activities with a constant rate of supply model. Cores with more than one rate have the rate of the entire core listed at the top of the cell with its varying rates throughout the core listed below. The rate of the entire core was calculated as a weighted average by year. For example, the mass and OC rate during interval C in UV2 remained constant for a longer period of time (Figure 1.5, Figure 1.6) than intervals A and B, and therefore was more heavily weighted in the average rate of the entire core. Letters A-C correspond to the intervals over which these rates were integrated in terms of mass and OC mass depth, as shown in Figure 1.5, Figure 1.6, and 0A1. In years: V1 A = 2020 – 1943.5 (76.5 y), B = 1943.5 – 1863.1 (80.5 y); V2 A = 2021 – 1945.7 (75.3 y), B = 1945.7 – 1865 (80.7 y); UV2 A = 2021 – 1999.6 (21.4 y), B = 1999.6 – 1991 (8.6 y), C = 1991 – 1895.6 (95.4 y).

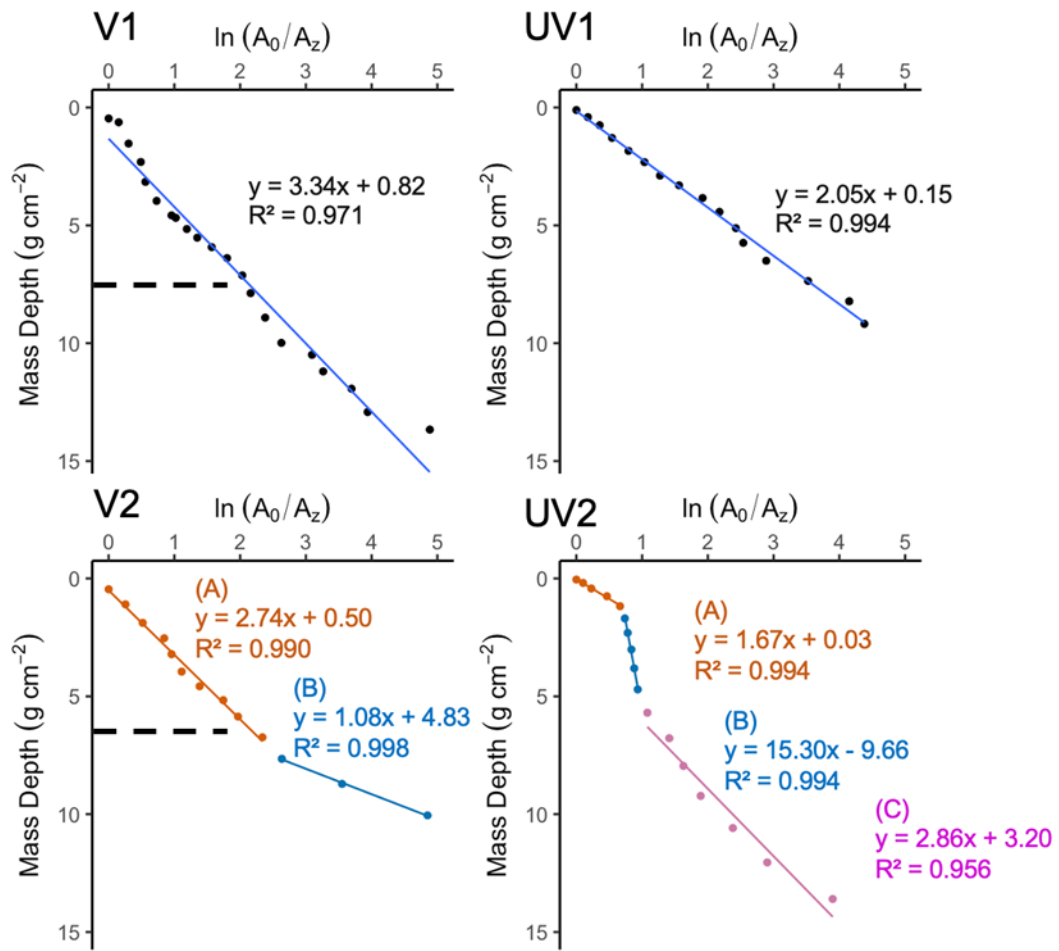


Figure 1.5: Unsupported ²¹⁰Pb activity vs. mass depth. Dashed lines indicate the bottom of the root zone in V1 (6.39 g cm⁻²) and V2 (7.65 g cm⁻²). Colors represent time periods of different mass accumulation rates. The line of best fit equation and R² value are listed and color-coded. Letters A, B, and C correspond to mass accumulation rates listed in Table 1.2.

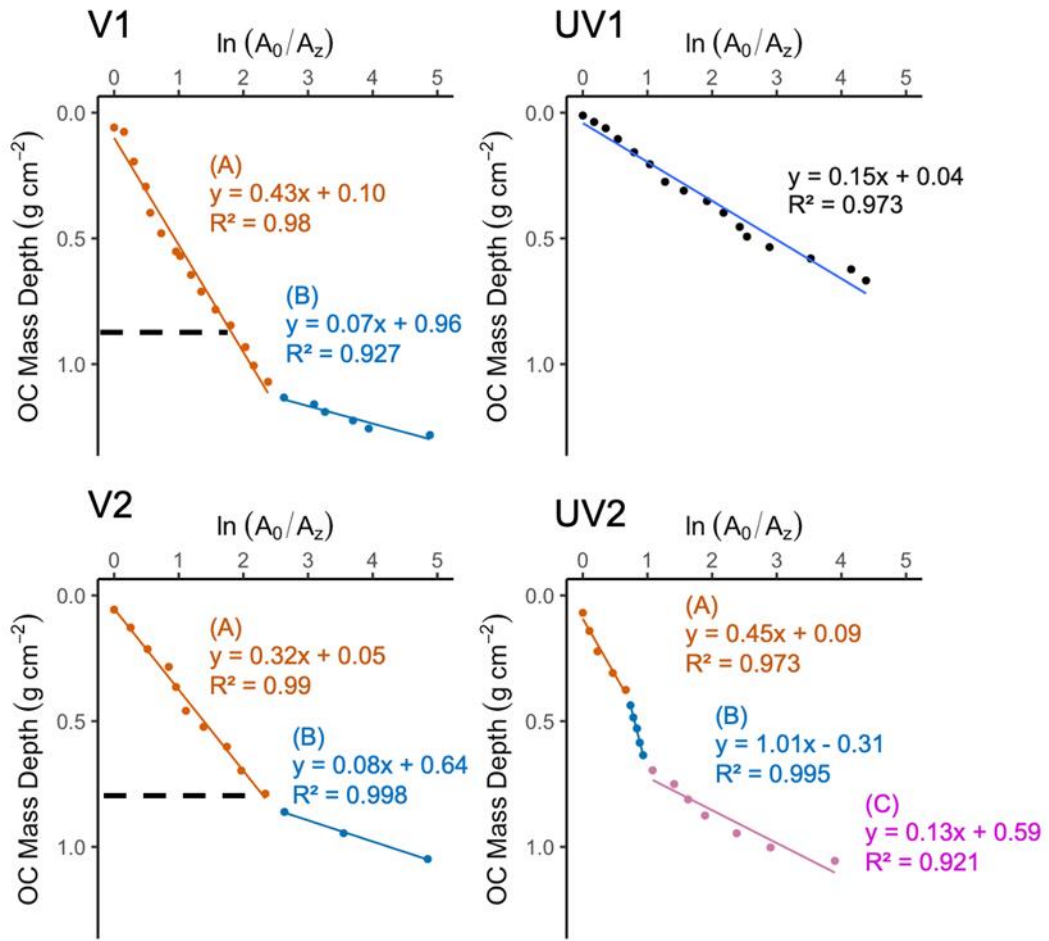


Figure 1.6: Unsupported ²¹⁰Pb activity vs. OC mass depth. Dashed lines indicate the bottom of the root zone in V1 (0.85 g cm⁻²) and V2 (0.86 g cm⁻²). Colors represent time periods of different OC accumulation rates. The line of best fit equation and R² value are listed and color-coded. Letters A, B, and C correspond to OC accumulation rates listed in Table 1.2.

Mass accumulation rates ranged from 584 ± 20.6 to 1091 ± 83.2 g m⁻² y⁻¹. V2 and UV2 showed histories of changing rates (Figure 1.5). Higher mass accumulation rates could indicate a time when the location was at a lower elevation or was vegetated. Lower elevation and/or *S. alterniflora* presence would promote higher sedimentation rates which would increase the mass accumulation rate. This idea is

supported by the fact that the surface rate in an unvegetated region in June (representative of the current vegetative state of this region; $UV2 = 520 \pm 22.9 \text{ g m}^{-2} \text{ y}^{-1}$; Figure 1.5) was lower than that of a vegetated region (representative of the current vegetative state of this region; $V2 = 851 \pm 30.2 \text{ g m}^{-2} \text{ y}^{-1}$; Figure 1.5). The same trend was found for the October cores ($V1 = 900 \pm 34.8$, $UV1 = 637 \pm 12.7 \text{ g m}^{-2} \text{ y}^{-1}$). In vegetated cores, the weighted average of both mass and OC accumulation rates were higher in October than in June ($V1 > V2$) by a factor of 1.5 and 1.2, respectively. This could be a result of seasonal differences in the quantities of OC in surface soils. Specifically, the amount of OC observed in marsh soils has been shown to vary throughout the year depending on the balance of production (release from belowground biomass, delivery via sedimentation) and removal (microbial remineralization and lateral hydrological transport) processes (Roman and Daiber 1989; Zhao et al., 2016; Vázquez-Lule and Vargas, 2021; Kayranli et al., 2010). The Senescent phenophase typically shows a peak in OC concentrations in the area above the root zone due to a release of OC from *S. alterniflora* into the soils, a process referred to as the “fall dump” (Schiebel et al., 2018). Much of this OC is labile and is removed throughout the Senescence and Dormancy phenophases when primary production rates are reduced and microbial and hydrological export processes dominate the OC mass balance in surface soils. This trend was not apparent in unvegetated cores where there is much less vegetative influence.

OC accumulation rates ranged from 48.1 ± 2.2 to $75.7 \pm 4.1 \text{ g m}^{-2} \text{ y}^{-1}$. $V2$ and $UV2$ showed a history of changing OC accumulation rates during the same periods of time when their mass accumulation rates varied (Figure 1.6). The highest OC accumulation rates throughout their histories ($V2$ (A) $103 \pm 3.5 \text{ g m}^{-2} \text{ y}^{-1}$; $UV2$ (B)

$313 \pm 12.5 \text{ g m}^{-2} \text{ y}^{-1}$) occurred during the same time as their highest mass accumulation rates (V2 (A) $851 \pm 30.2 \text{ g m}^{-2} \text{ y}^{-1}$; UV2 (B) $4757 \pm 209 \text{ g m}^{-2} \text{ y}^{-1}$), suggesting that the sedimentation rate (inorganic + organic) was proportional to the OC accumulation rate. However, the second-highest mass accumulation rate throughout UV2 (UV2 (C) $889 \pm 85.4 \text{ g m}^{-2} \text{ y}^{-1}$) did not occur at the same time as its second-highest OC accumulation rate (UV2 (A) $140 \pm 13.3 \text{ g m}^{-2} \text{ y}^{-1}$) indicating that during UV2 (C) (1986.3 – 1895.6), there was either a relatively higher ratio of inorganic to organic input or a relatively higher rate of OC decomposition. V1 also showed a history of varying OC accumulation rates albeit not reflected in the mass accumulation rate. The OC accumulation rates in vegetated cores were higher than unvegetated cores in October (V1 = $75.7 \pm 4.1 > \text{UV1} = 48.1 \pm 2.2 \text{ g m}^{-2} \text{ y}^{-1}$) but not June (V2 = $63.0 \pm 2.3 < \text{UV2} = 76.2 \pm 0.2 \text{ g m}^{-2} \text{ y}^{-1}$). The rates of the October cores were higher than those of the June cores in vegetated (V1 = $75.7 \pm 4.1 > \text{V2} = 63.0 \pm 2.3 \text{ g m}^{-2} \text{ y}^{-1}$) but not unvegetated regions (UV1 = $48.1 \pm 2.2 < \text{UV2} = 76.2 \pm 0.2 \text{ g m}^{-2} \text{ y}^{-1}$).

Figure 1.7 compares the OC accumulation rates of all cores calculated using varying ^{210}Pb -based timescales as follows: 1) 30 years (providing a low-endmember timescale), 2) 58 years (to compare to ^{137}Cs -based rates), 3) 100 years (the timescale used by greenhouse gas inventory reports following global warming potential (GWP) reporting standards in the IPCC Fifth Assessment Report, 2014 (AR5); Crooks et al., 2018; Najjar et al., 2018; Holmquist et al., 2018), and 145 years (bottom of the dated cores). When integrated over longer timescales, OC accumulation rates not only decreased but approached agreement, as shown by the decreasing relative standard deviation between all four cores (Table 1.4), a demonstration of the “Sadler effect.”

This indicates that vegetation presence and the *S. alterniflora* phenophase (which control differences in surface soil OC concentrations; Figure 1.4) affect OC accumulation rates on shorter timescales and become less influential over longer timescales when OC from deeper soil regions is taken into account. This can be explained by the high ratio of labile to recalcitrant C at the surface of salt marsh soils. Labile OC is remineralized throughout a core, but at depth these remineralization processes dominate because there are no new OC inputs from vegetation below the root zone. Thus, at depth, this labile to recalcitrant OC ratio (and total OC) declines. As the timescale of interest increases (generally correlated with depth), the percent of labile OC decreases.

The trend of declining OC accumulation rates with longer timescales of integration was most apparent in V1 and UV2. It was unexpectedly much more apparent in the unvegetated (UV2) than the vegetated (V2) core in June and UV1. UV2 shows a high OC accumulation rate from 1991 to 1997.3 (UV2 (B); Table 1.2, Figure 1.6) that skews the 30 and 50 year estimates (Figure 1.7) towards higher values, making the aforementioned trend more apparent. In theory, this trend is expected to be more apparent in vegetated cores due to vegetative inputs, especially when comparing timescales of <150 years. However, OC accumulation rates may vary over time as a result of changing marsh conditions, muddling the effects of vegetation, as is the case with UV2. Generally speaking, the decrease in OC accumulation rates over depth/time in cores V1, V2, and UV2 (Table 1.2) further explain why OC accumulation rates averaged by year decrease with increasing timescale (Figure 1.7). The Sadler effect would likely be observed in UV1 as well if OC accumulation rates over millennial timescales were available (DeLaune et al., 2018; Tucker, 2016; Zehetner, 2010).

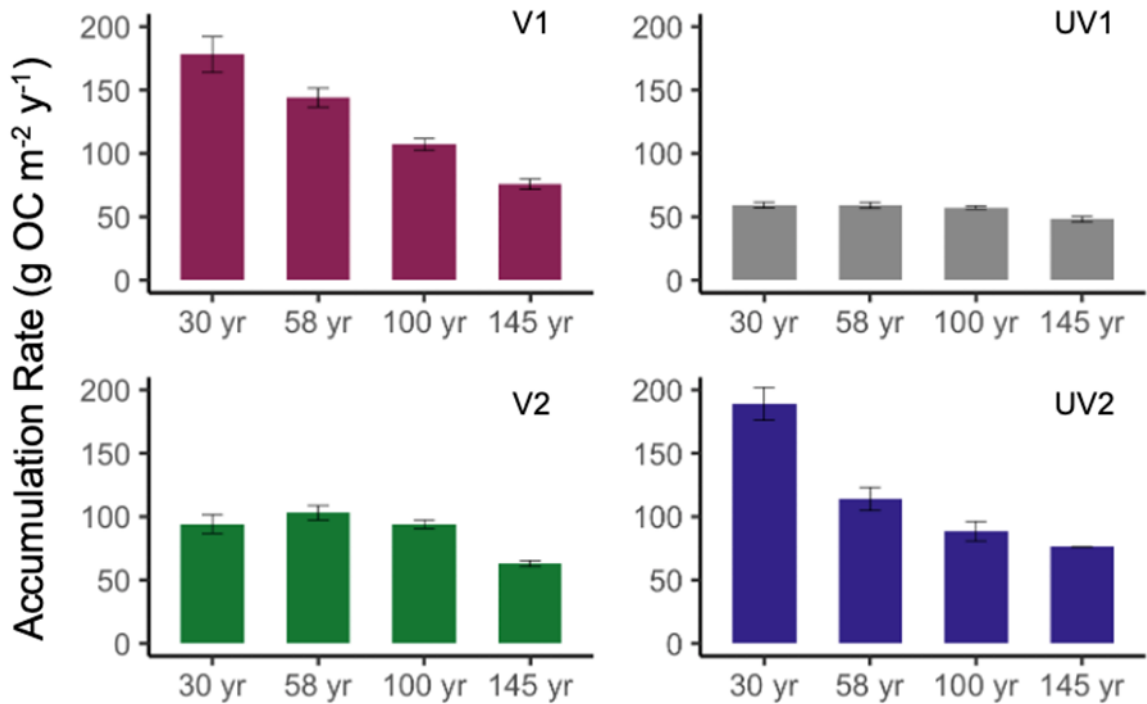


Figure 1.7: OC accumulation rates over varying timescales calculated using ²¹⁰Pb-dated soils. October vegetated (maroon) and unvegetated (gray), June vegetated (green) and unvegetated (blue) cores are separated to highlight differences within each core.

Longer, centennial timescales that incorporate a greater fraction of refractory, accumulated OC and a lower fraction of labile, seasonally cycling OC are more useful and accurate for calculating accumulation rates. A true accumulation rate must incorporate both C inputs and losses. ¹³⁷Cs dates soils only as far back as 1963 while ²¹⁰Pb dates soils 100-200 years prior to sampling (Wallbrink et al., 2002; Yuknis 2012). In this study, ¹³⁷Cs dating limited the timescale to 57-58 years or depths of 25.2 to 37.3 cm (Table A2). Importantly, the depth profiles for soil OC show these depths to be within or just below the root zone and above the area where OC decline stabilizes OC inventories at lower concentrations (Figure 1.4). Thus, while a ¹³⁷Cs-

derived C accumulation rate incorporates the C added to the top of the core, it neglects losses of soil OC to remineralization processes below the root zone. The ^{210}Pb approach dated soils to 144 ± 15 years, or 32.5-61.5 cm depth (Table 1.3), an area that extends below the root zone and captures some of these OC losses (Figure 1.4). Thus, not only are the shorter cores subject to issues related to the vegetative phenophase at core collection and the presence or absence of vegetation, but they also neglect OC losses that need to be accounted for to calculate true accumulation rates. Subsequently, longer, centennial timescales are needed to accurately reflect the value of these blue C ecosystems for the purposes of removing CO_2 from the atmosphere. Because they are benchmarked to 1963, older studies using ^{137}Cs dating have been limited to even shorter, decadal timescales than those described here, and previously estimated C accumulation rates should be viewed with caution. As a result, studies that use timescales of <50 years may end up overestimating the OC accumulation rate.

An additional problem exists with the intercomparability of dates derived from the ^{137}Cs and ^{210}Pb markers which do not always yield equivalent dates at the same depth. For example, soils at 27.3 cm in V2 were dated to 58 years with ^{137}Cs and 84.8 years with ^{210}Pb (Table 1.3, Table A2). The 1963 ^{137}Cs peak showed up at the 1955, 1936, and 1986 ^{210}Pb -based depths in cores V1, V2, and UV2, respectively (Table A2). This may be a result of ^{137}Cs and ^{210}Pb mobility within the sediment (Drexler et al., 2017) and could be an indication of the waning utility of ^{137}Cs over time (Drexler et al., 2018).

Table 1.3: OC accumulation rates of all 4 cores integrated over varying timescales. 57 and 58-year timescales were obtained using ^{137}Cs . 31.2 ± 1.4 , 59.1 ± 2.6 , 92.6 ± 6.0 and 144 ± 15 -year timescales were obtained using ^{210}Pb . ^{210}Pb -based accumulation rates are reported as yearly weighted averages.

Core	Method	Timescale (y)	Soil Depth (cm)	OC accumulation rate ($\text{g m}^{-2} \text{yr}^{-1}$)
V1	^{210}Pb	30.7	19.5	178 ± 14.1
	^{210}Pb	57.8	34.5	144 ± 7.5
	^{137}Cs	57	37.5	163.5
	^{210}Pb	99.3	49.5	107 ± 4.7
	^{210}Pb	157	61.5	75.7 ± 4.1
UV1	^{210}Pb	33.3	16.5	59.3 ± 2.3
	^{210}Pb	61.7	25.5	59.1 ± 2.4
	^{137}Cs	57	n.d.	n.d.
	^{210}Pb	92.7	37.5	57.4 ± 1.2
	^{210}Pb	141	46.5	48.1 ± 2.2
V2	^{210}Pb	30.8	11.7	94.2 ± 7.5
	^{210}Pb	56.1	19.5	103 ± 5.7
	^{137}Cs	58	27.3	148.4
	^{210}Pb	84.8	27.3	94.0 ± 3.3
	^{210}Pb	156	32.5	63.0 ± 2.3
UV2	^{210}Pb	30	22.8	189 ± 13
	^{210}Pb	60.8	32.4	114 ± 9.1
	^{137}Cs	58	25.2	119.9
	^{210}Pb	93.4	37.2	88.4 ± 7.8
	^{210}Pb	125.4	39.6	76.2 ± 0.2

Table 1.4: Relative standard deviations of the OC accumulation rates of all 4 cores over different ^{210}Pb -based timescales.

Timescale (yr)	Relative Standard Deviation of OC Accumulation Rates
30	0.49
58	0.33
100	0.24
145	0.20

Most blue C budget studies use ^{137}Cs and marker horizon-based timescales to date soils and calculate OC burial rates (Ouyang and Lee, 2014). Table 1.5 compares OC accumulation rates from this study to a similar study conducted by Tucker (2016) in the Great Marsh as well as average NW Atlantic regional and global rates, as reported by Ouyang and Lee (2014). The ^{210}Pb -based average OC accumulation rate of the cores in this study ($65.7 \pm 13.3 \text{ g m}^{-2} \text{ yr}^{-1}$; 144 ± 15 -year timescale) was not within range of the rates reported by most other studies. The ^{137}Cs -associated rate, however, was ($144 \pm 22 \text{ g m}^{-2} \text{ yr}^{-1}$). This indicates that OC accumulation rates that have been calculated using different radionuclides are not necessarily comparable. The ^{137}Cs -associated rates reported in this study were within range of previously reported rates from the Great Marsh and average NW Atlantic rates but not global rates, which are much higher. Both the NW Atlantic average rates and rates reported in this study are lower than the global average possibly due to the Great Marsh and NW Atlantic sites having lower latitudes ($35\text{-}46.4^\circ\text{N}$) than those associated with the highest reported OC accumulation rates ($48.5\text{-}58.5^\circ\text{N}$; Ouyang and Lee, 2014).

Table 1.5: Comparison of OC accumulation rates of this study to regional and global rates.

Source	Dating method	Timescale (yr)	Study site	OC accumulation rate (g m ⁻² yr ⁻¹)
This study	²¹⁰ Pb	144 ± 15	Great Marsh, DE	65.7 ± 13.3
This study	¹³⁷ Cs ¹	57, 58	Great Marsh, DE	144 ± 22
Tucker, 2016 (cores sampled in 2007, 2014)	¹³⁷ Cs	44, 51	Great Marsh, DE	121.0 ± 23.4
Ouyang and Lee, 2014	¹³⁷ Cs and marker horizons ²	≤ 48	NW Atlantic	134.0 ± 12.8 ⁴
Ouyang and Lee, 2014	¹³⁷ Cs and marker horizons ²	≤ 50	Global average	244.7 ± 26.1 ⁴

¹Only 3 out of 4 cores in this study had a ¹³⁷Cs peak.

²Marker horizons are another common tool used to date soils. This method uses feldspar clay to date short-term sedimentation (Morris and Callaway, 2018).

³Calculated using data provided by Ouyang and Lee (2014). Averaged over the number of studies reported, not weighted by regional area coverage.

⁴Weighted average by regional area coverage, reported by Ouyang and Lee (2014).

Although salt marshes are understood as being physically heterogeneous (i.e. in terms of tidal influence, water table depth, microbial activity; Seyfferth et al., 2020) which leads to soil OC heterogeneity (Zhao et al., 2016), these data suggest that salt marsh soil OC quantities become increasingly homogenous with depth. The OC accumulation rate estimate of a salt marsh becomes more accurate as the timescale increases and as more variations in burial rate over time are included in the average reported rate. I show that the timescale, dating method, season of collection, location of collection, and soil OC depth profile are all critical to report in tandem with any salt

marsh OC accumulation rate. Similarly, papers that synthesize regional or global data should include the methods and timescale used in any one study so that readers may assess the comparability of the reported rates. If OC accumulation rates are to be used to quantify salt marsh CO₂ removal from the atmosphere, any OC additions to soils in the surface must be balanced by the apparent losses just below the root zone where OC concentrations in the 4 cores from this study show clear declines. Collecting cores of at least 50 cm would effectively satisfy this recommendation, as shown by soil OC profiles in this study (Figure 1.4) and previous works (Mueller et al., 2019; Van de Broek et al., 2016; Tucker, 2016). This would require studies that intend to report salt marsh OC accumulation rates to 1) report soil OC profiles and 2) use radionuclides other than ¹³⁷Cs to date soils, such as ²¹⁰Pb and/or ¹⁴C, depending on the maximum depth of detectable unsupported ²¹⁰Pb activity. ¹³⁷Cs is additionally limited as a dating tool because it can only be used to calculate a single rate between the date of collection and 1963 and therefore cannot be used to identify variations in accumulation rates over that time period. ¹³⁷Cs-derived rates have also been suggested to be of waning utility over time in previous work (Drexler et al., 2018). In this study, ²¹⁰Pb dated soils older than 1963 (¹³⁷Cs limit), but was not always effective in dating soils to this 50 cm depth at which a net C balance was met (i.e., V2; Table A2), therefore an additional radionuclide with a longer half-life may be needed to date soils in some cases. Additionally, if the research question at hand requires using relatively shallow depths and short timescales (i.e., to estimate anthropogenic sea level rise-induced C burial changes over decadal timescales), then this 50 cm recommendation becomes irrelevant. Standardizing the approach to calculating and reporting OC accumulation in the blue C community may be challenging but would improve current

regionally and globally reported rates and our overall understanding of salt marsh carbon storage potential.

1.3.3 Composition of OM Pools

1.3.1 and 1.3.2 describe the OM depth profiles of the Great Marsh and the rates at which OC has been buried in its soils over the last ~145 years. Previous studies have shown that OM composition can impact the fate of OM in the environment (Morris and Callaway, 2018; Unger et al., 2016; Enríquez et al., 1993; Burdige, 2007) including its preservation. Here, I characterize the OM composition over depth of the core soils and porewaters to provide perspectives on how the OM composition changes over the three depth ranges of interest (the surface/root zone, the remineralization zone, and the burial zone) and to attempt to understand the mechanisms driving OC burial in this salt marsh.

1.3.3.1 ^{13}C NMR

Salt marsh bulk soil signals at the surface resemble degraded *S. alterniflora* ^{13}C NMR spectra (Figure 1.8; Liu et al., 2021) while the HA ^{13}C NMR spectra show similar features to those reported in other soil HA studies (Figure 1.9; Santín et al., 2008; Adani et al., 2006; Mao et al., 2000). ^{13}C NMR signals were integrated using the regions and peak assignments specified in Table 1.6 and Table 1.7 following assignments used in previous solid state multi-CP and DP MAS ^{13}C NMR studies analyzing natural soil and water samples (Santín et al., 2008; Wozniak et al., 2020; Adani et al., 2006; Witte et al., 1998; Mao et al., 2000; Abdulla et al., 2010). Carbon associated with alkyl, O-alkyl, and aromatic groups were the most prominent moieties found in both HA and bulk soil spectra (Figure 1.10). Compared to bulk soils, HAs

had a higher mean relative abundance of carboxyl/amide-C ($4 \pm 1\%$), aromatic-C ($12 \pm 1\%$), and N-alkyl/methoxy-C ($2 \pm 0.5\%$), a lower relative abundance of O-alkyl-C ($17 \pm 4\%$), and similar amounts of alkyl-C, averaged over all depths and cores (Figure 1.10). Most peaks listed in Table 1.7 are observed in every HA spectrum (Figure 1.9). The peak at 22 ppm representing CH₃ groups only appeared in the HA of UV1 suggesting a loss of these terminal methyl functional groups with depth and diagenesis. Compared to HAs, bulk soil spectra contained less relative signal from aromatic and carboxyl/amide-C and an additional O-alkyl peak at 104 ppm in all cores at most depths (Figure 1.8). In the surface/root zone of vegetated and unvegetated cores, HAs in June contained 7% and 3% more O-alkyls than HAs in October, respectively (Figure 1.10) suggesting that the higher *S. alterniflora* productivity in June releases carbohydrate-like OM into surface soils. Additionally, the broad peaks in bulk soils and V1 humic acids could be due to the presence of Fe²⁺ and Fe³⁺, which could suggest Fe-HA complexation.

Table 1.6: Chemical shift assignments for integrated regions observed in ¹³C NMR data.

Functional Group	Integrated Region (ppm)
Alkyl C	0-45
N-alkyl C, methoxy C	45-60
O-alkyl C	60-110
Aromatic C	110-160
Carboxyl, amide C	160-185
Carbonyl C	185-220

Table 1.7: Chemical shift assignments for peaks observed in ^{13}C NMR data.

Letter Denotation	Moiety	Chemical Shift (ppm)
i	CH ₃ , short-chained/branched alkyl	22
ii	CH ₂ , long chain alkyl	30, 33
iii	Methoxy	54, 56
iv	N-, O-alkyl on aromatic moiety, carbohydrates	71, 104
v	Aromatic	115, 126, 128, 131, 132
vi	Lignin, tannin	148, 153
vii	Carboxyl	173

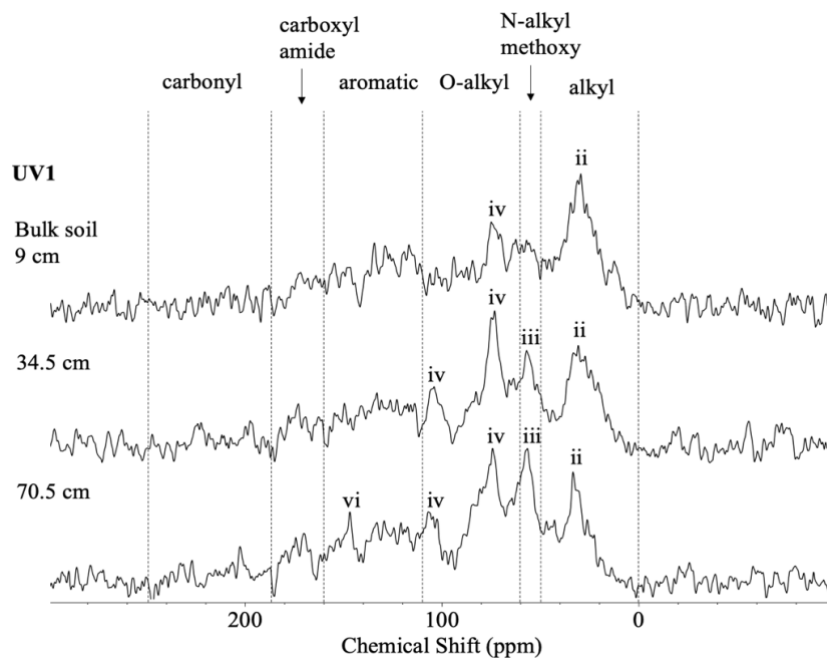
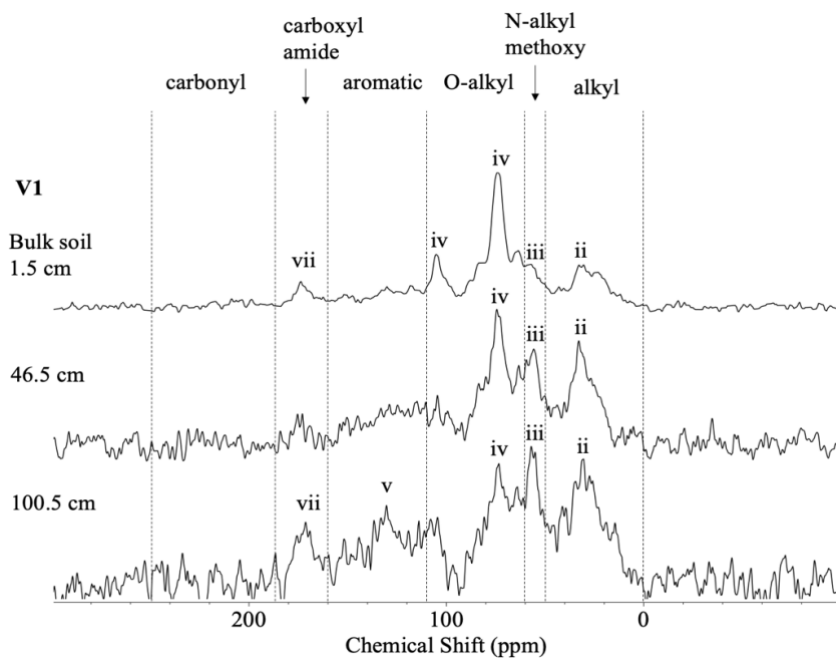


Figure 1.8: ^{13}C NMR signals of bulk soils from the surface/root, remineralization, and burial zones from all cores collected in October 2020 and June 2021. The peak labels correspond to chemical shift assignments described in Table 1.7.

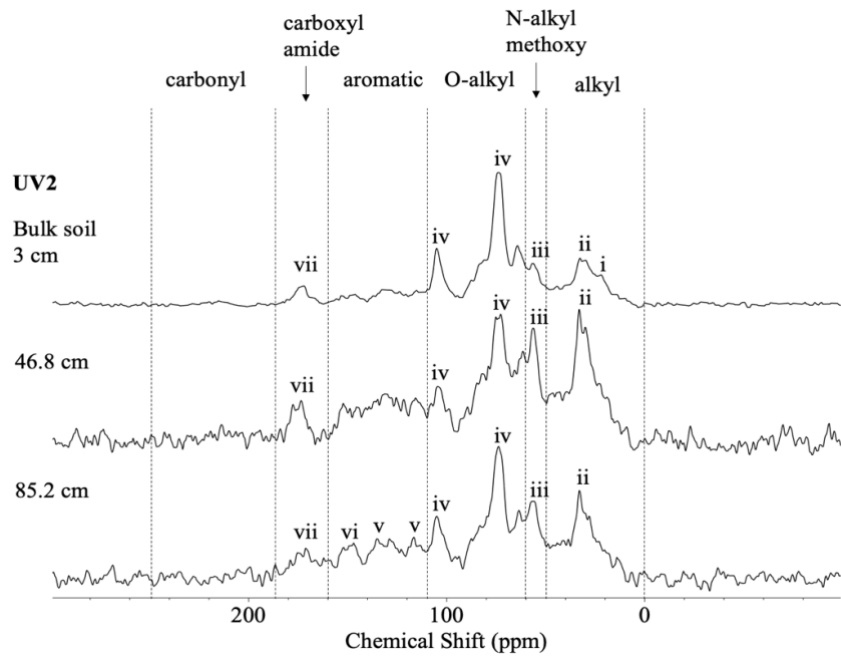
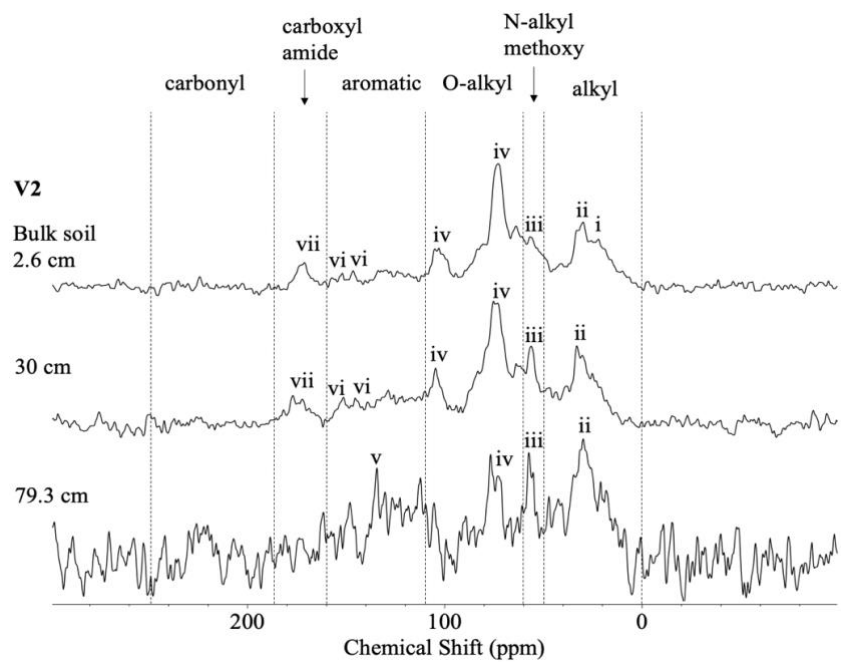


Figure 1.8: continued.

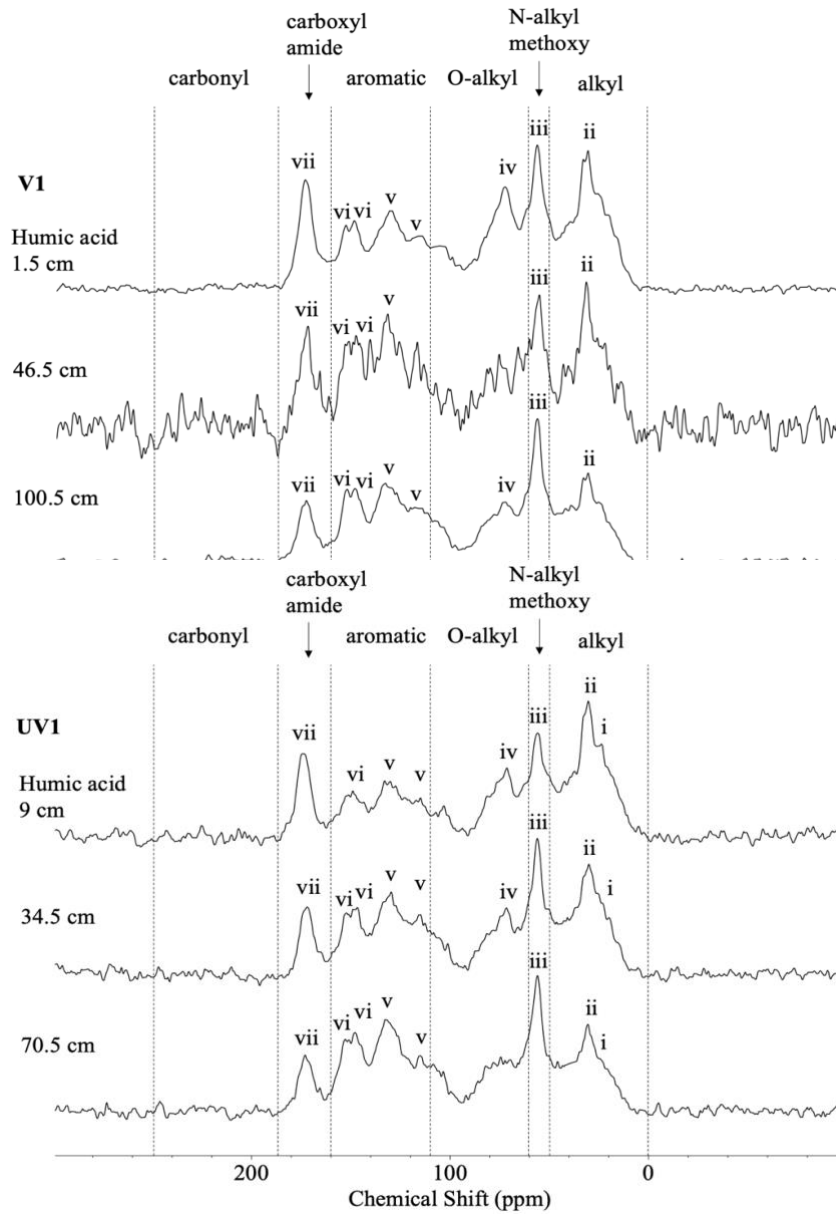


Figure 1.9: ^{13}C NMR signals of humic acid from the surface/root, remineralization, and burial zones from all cores collected in October 2020 and June 2021. The peak labels correspond to chemical shift assignments described in Table 1.7.

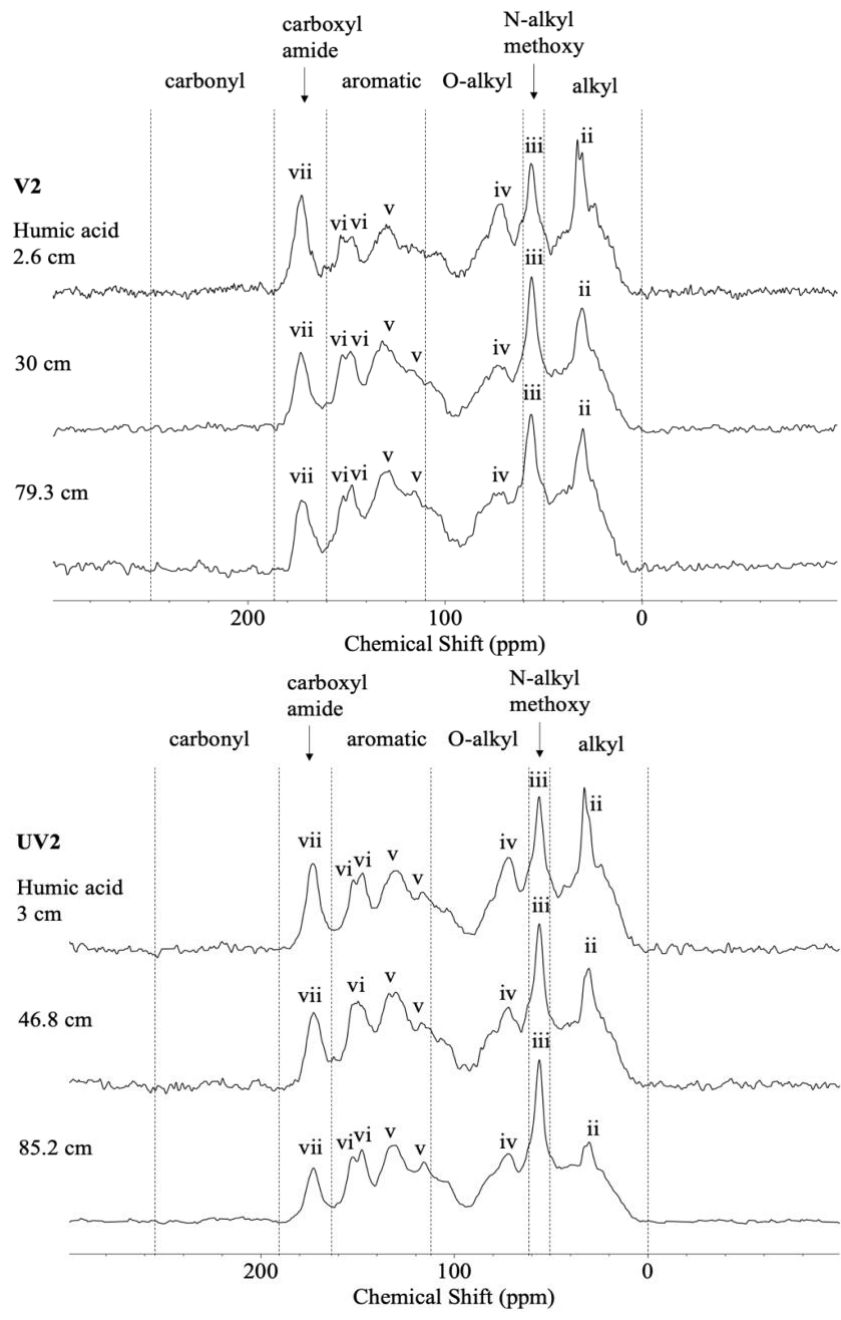


Figure 1.9: continued.

There were distinct trends with depth in both the bulk soil and HA (Figure 1.10). In bulk soils, the relative contributions from aromatic C increased by $9 \pm 7\%$ on average over depth in all cores. The relative contribution of O-alkyl carbons, in contrast, decreased with depth (decrease from surface to depth averaged over all cores = $12 \pm 15\%$) in all cores. Aromatic compounds have been shown to increase in relative abundance by various amounts compared to other carbonaceous moieties with increasing OM decomposition, an observation leading to the conclusion that these compounds may be inherently resistant to degradation and therefore selectively preserved (as observed in soil biochars by Kuzyakov, 2014). This could be due to the inability of the microbes in the soil to metabolize aromatics or that aromatics contain carboxylic acid or hydroxyl functional groups that allow them to associate with minerals relatively well, both of which would preclude degradation (Burdige, 2007; Kaiser and Guggenburger, 2000). 20-30% decreases in soil O-alkyl or carbohydrate C content have been attributed to their relatively higher microbial lability (Hatcher et al., 1983), and their decline with depth in these cores suggest their preferential remineralization over time.

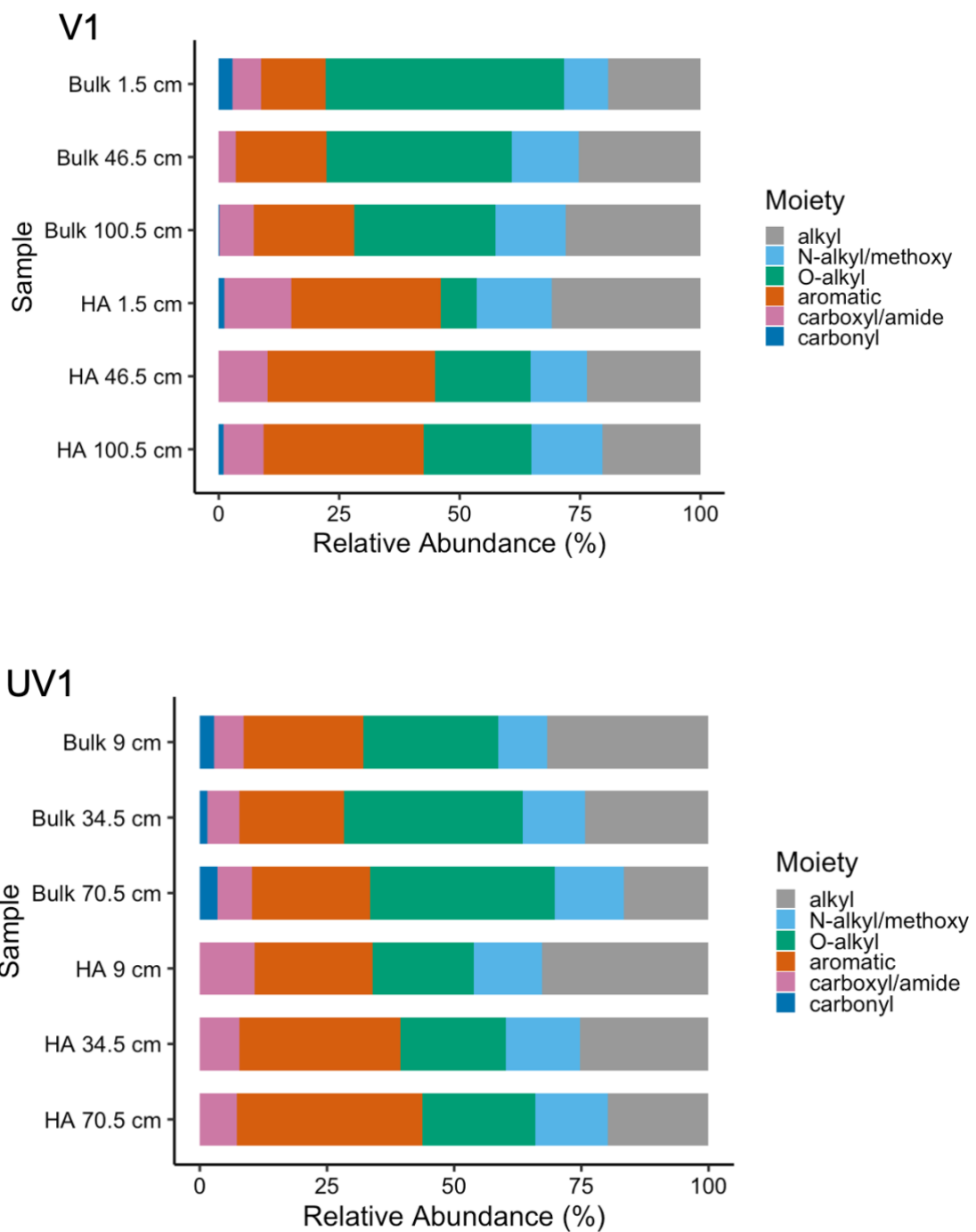


Figure 1.10: Relative abundances of functional groups detected in ^{13}C NMR spectra and integrated for regions defined in Table 1.6. The core ID is denoted in the upper left corner of each bar plot. Within each core, data from bulk soil and HA surface, mid-depth, and deep sections are displayed.

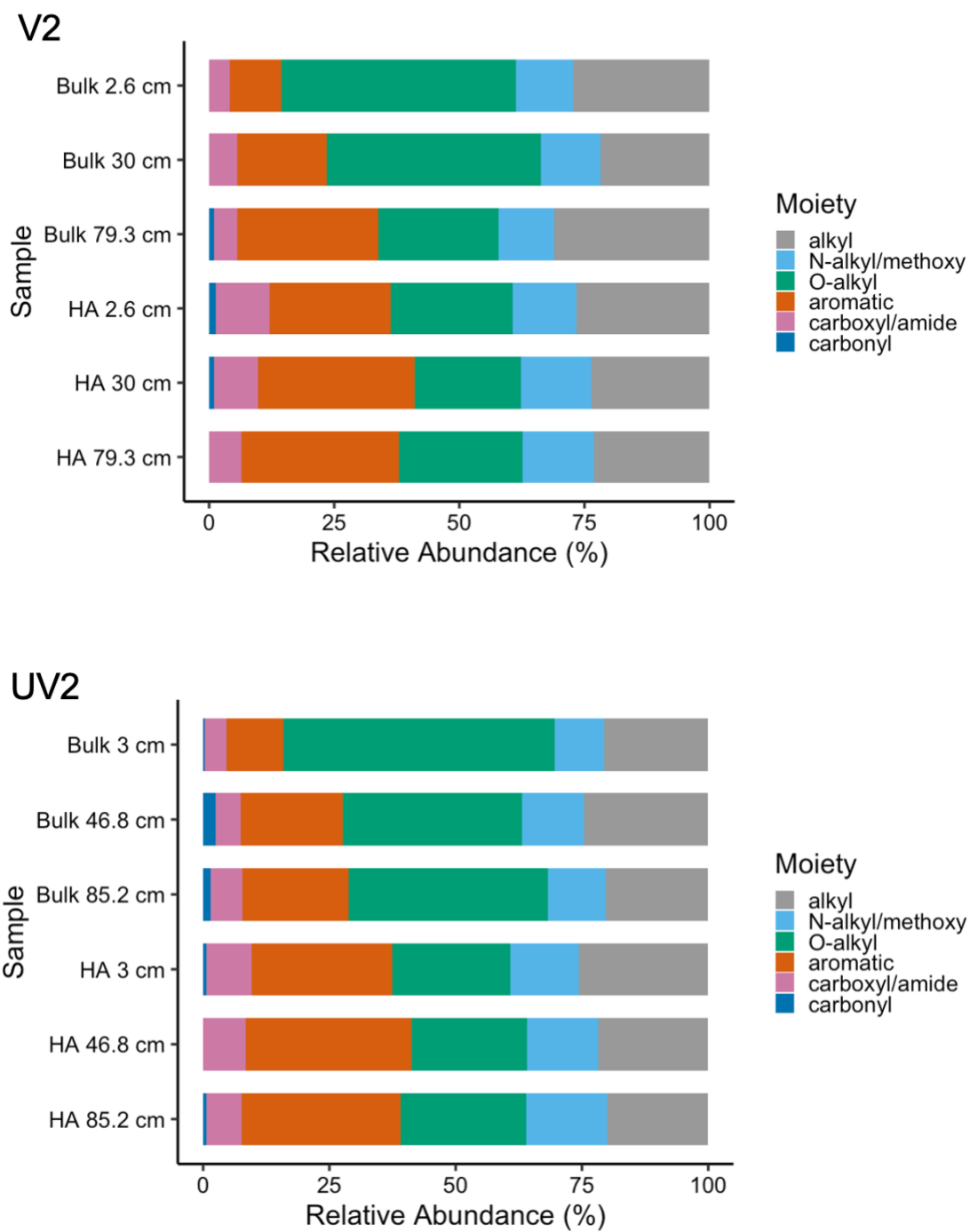


Figure 1.10: continued.

From the surface to depth, HA carboxyl/amide and alkyl-C groups decreased by $4 \pm 1\%$ and $8 \pm 4\%$, respectively, with depth while aromatics increased by $7 \pm 5\%$ (Figure 1.10). The decrease in relative carboxyl/amide abundance and increase in relative aromatic-C abundance over depth is consistent with previous observations of tropical soils (Zech et al., 1997). Increasing aromatic character is indicative of increasing humic content over depth, a theory that is supported by the observed increase in the humic C/bulk soil OC ratio with depth (Figure A3). In contrast to the trends observed here, alkyl (or aliphatic) C has been previously shown to accumulate in humic and fulvic acids over depth in NE Atlantic salt marshes (Santín et al., 2008) and have been understood as being a signature component of HAs in general (Filip et al., 1988; Zech et al., 1997). The differences in relative aliphatic content may relate to the unique NW Atlantic salt marsh environment and vegetative communities. On the other hand, aquatic HAs have more aliphatic content than soil HAs (Thorn et al., 1989). Mao et al. (2007) observed 45.5% aliphatic content in estuarine water HA while Santín et al. (2008) and the data in this study show 20-30% aliphatics in salt marsh soil HA. This previously unobserved (to the best of my knowledge) drop in alkyl content with depth in HA could reflect strong tidal contributions at the surface that are removed via remineralization with depth, leaving higher contributions from salt marsh soil OM at depth. Additionally, the concomitant decrease in alkyl and carboxyl/amide content with depth could indicate the decrease of carboxyl-containing aliphatic molecules (CCAM), a signature component of soil HAs that has been identified in highly humified forest, swamp forest and open field soils by FTICR-MS (DiDonato et al., 2016). A decrease in HA CCAM could therefore indicate decomposition of these moieties. The decrease in HA carboxyl/amide-C could also

represent the degradation of amide functional groups. This carboxyl/amide-C region of the ^{13}C NMR spectrum represents a combination of two C moieties which makes it difficult to parse which trends are occurring. Further molecular level analyses (via FTICR-MS or another technique) are needed to evaluate these hypotheses.

Figure 1.11 shows how the relative abundances of functional groups compare within the surface/root zone and within the burial zone across all cores. Qualitatively within each pool, bulk soils and HAs were more variable in the surface than in the burial zone. Comparing the two pools, bulk soils and HAs were more structurally similar in the burial zone than at the surface. In other words, the OM composition of HA and bulk soil pools both individually and combined became more homogeneous over depth. In the surface zone, HA carboxyl/amide, aromatic, and O-alkyl groups were on average 6% higher, 12% higher, and 25% lower than the content in bulk soils, respectively (Figure 1.10). At depth, these differences become 0%, 3%, and -4%, respectively. Thus, the bulk soils became increasingly similar in structure to HAs with depth independent of vegetation and season. Hatcher et al. (1983) made similar observations for lacustrine sapropels in which the OM structural changes with depth were more drastic than their humin counterparts and became increasingly similar in structure to the humin itself. The increasing similarity between the HA and bulk soil OM ^{13}C NMR spectra also supports the argument that humic acids are accurate representations of refractory organic matter pools in that the extraction process does not artificially alter the natural makeup of the starting material (Olk et al., 2019). Other, more detailed analyses are needed to understand which mechanisms cause the chemical composition of these OM pools to become so similar over the course of burial.

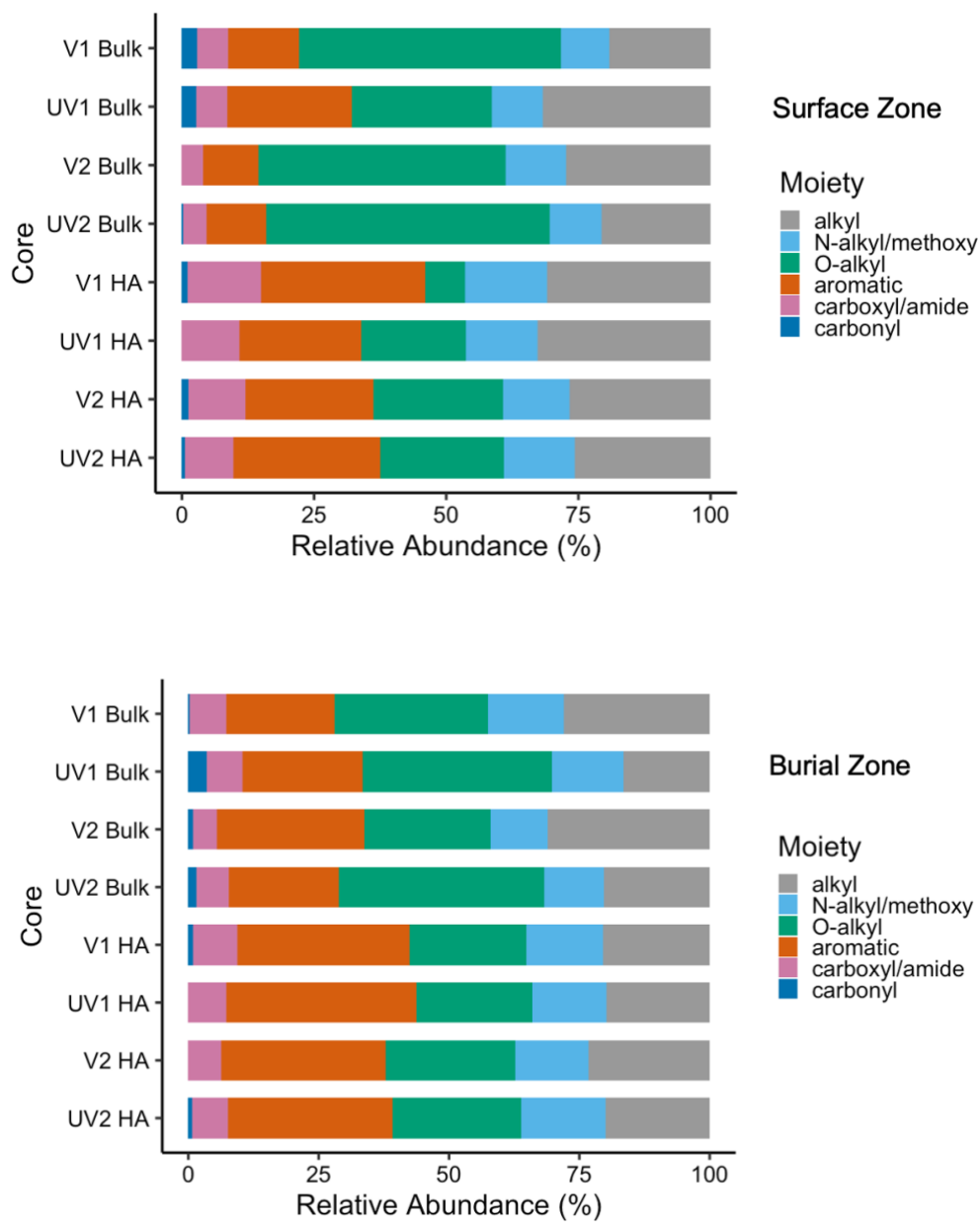


Figure 1.11: Relative abundances of functional groups detected by ^{13}C NMR signals and integrated by regions defined in Table 1.6. The surface (top) and burial (bottom) zones of bulk soil and HA from all cores are compared to show increasing compositional homogeneity with depth.

1.3.3.2 Porewater DOC and EEMs

Porewater DOC also reflected vegetative influence at the surface which decreased in the remineralization zone (Figure 1.12). Roots in vegetated cores absorb water well which made it difficult to extract porewater from root-dense sections. As a result, there was limited porewater data at the surface of vegetated cores. Vegetated cores in both October and June had higher surface DOC concentrations than unvegetated cores in the same season, implying contributions related to newer *Spartina* biomass. V2 showed higher surface porewater DOC concentrations (10.6 ± 8.0 mM) than V1 (6.89 ± 0.7 mM), possibly due to higher productivity in June resulting in higher total soil OC concentrations observed in the root zone (Figure 1.4). DOC concentrations dropped in both V1 and V2 around the bottom of the root zone, reflective of the observed lower soil OC mass concentrations in the remineralization zone (Figure 1.4) and the associated decrease in the influence of *Spartina* biomass. Porewater DOC concentrations in unvegetated cores were low at the surface (likely reflecting the lack of new plant biomass) and increased with depth before converging to concentrations of 3.5-5 mM DOC. Thus, surface porewater DOC chemistry appears to be influenced by vegetative and seasonal variations at the surface but not at depth.

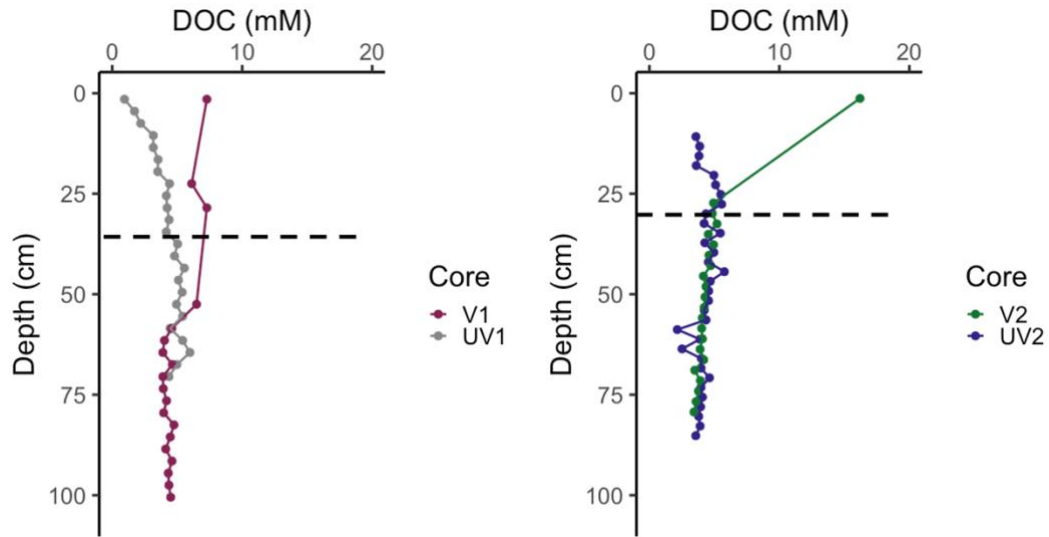


Figure 1.12: Porewater DOC depth profiles of October (left) and June (right) cores. Dashed lines indicate the bottom of the root zone in V1 (34.5 cm) and V2 (27.3 cm).

As total soil OC concentrations declined with depth, porewater HIX values increased (Figure 1.14). A positive correlation was observed in UV1 ($R = 0.83$, $p < 0.001$) and V2 ($R = 0.80$, $p < 0.001$; Figure 1.14), an observation that is consistent with OC exchange between soil and porewater. As a labile fraction of soil OC is remineralized, the remaining OC is selectively preserved and/or humified. Hydrophilic, humified OC in the soil may then be transferred to the FDOM pool in the presence of water. Such a transfer of humified OC to the dissolved phase is consistent with the increase in porewater FDOM HIX values observed here.

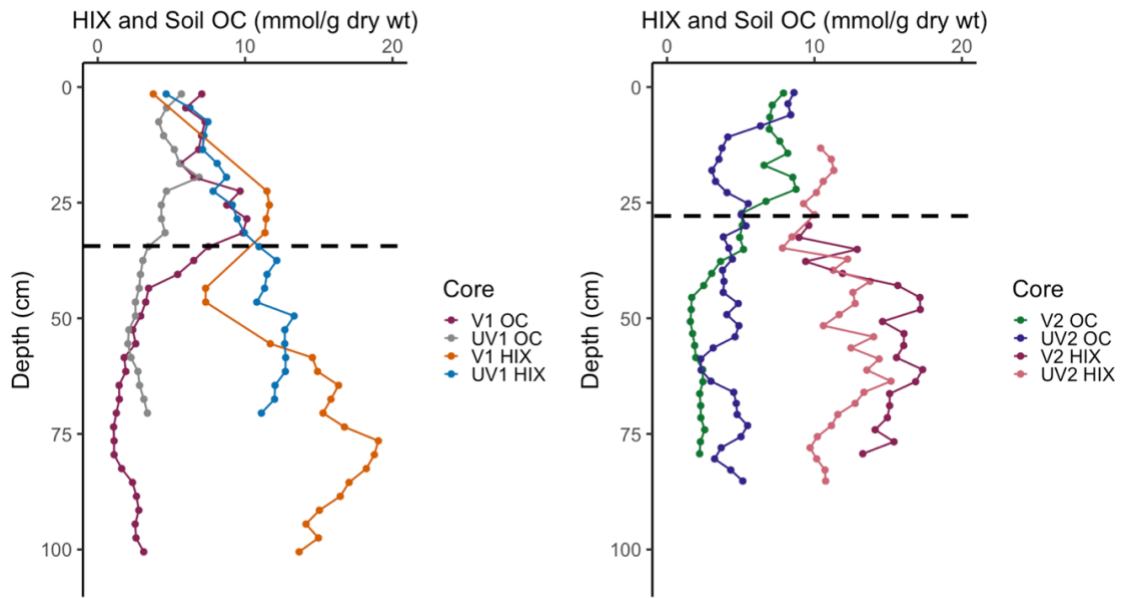


Figure 1.13: Soil OC and porewater HIX depth profiles taken from cores in October 2020 (left) and June 2021 (right). Dashed lines indicate the bottom of the root zone in V1 (34.5 cm) and V2 (27.3 cm).

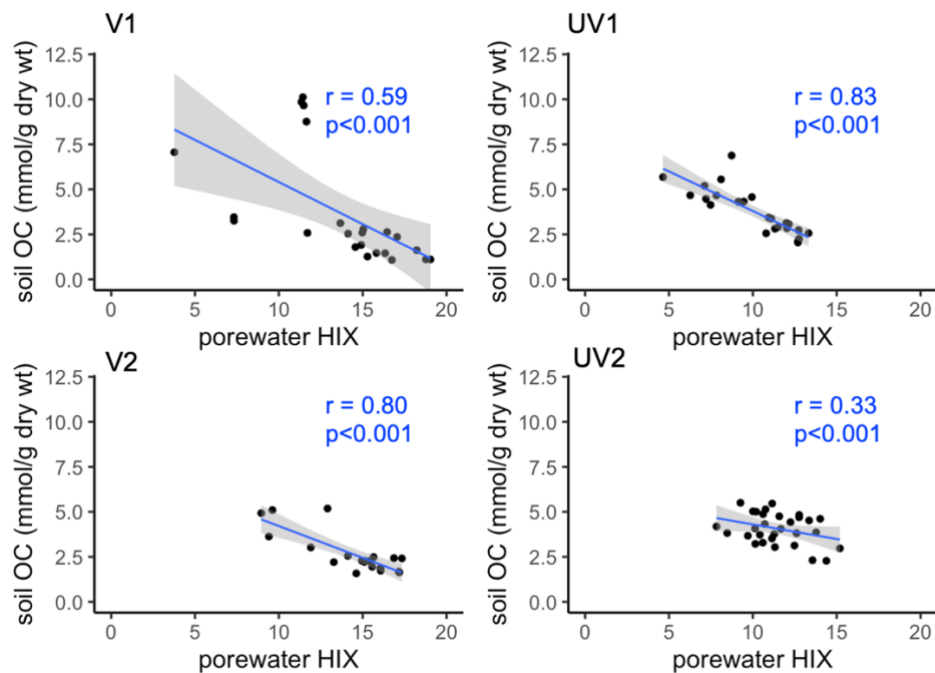


Figure 1.14: Correlations between soil OC and porewater HIX.

1.3.3.3 Sulfurized OM

The HA C/S depth profile is shown in Figure 1.15. This ratio decreased by a factor of 10-100 over depth in cores V1 and V2 but did not show any trends in cores UV1 or UV2. A drop in the HA C/S ratio over depth could indicate the occurrence of sulfurization, as observed by Ferdelman et al. (1991) in the Great Marsh. Sulfurization is defined as the reaction between organic matter and reduced inorganic sulfur which produces organic sulfur compounds. It has been observed in euxinic (sulfidic and anoxic) environments such as salt marshes, anoxic basins, and hydrothermal vents (Ferdelman et al., 1991; Raven et al., 2016; Gomez-Saez et al., 2016). Sulfurized organic matter has been shown to be preferentially preserved in these euxinic environments (Raven et al., 2016; Yücel et al., 2010; Henneke et al., 1997). A decreasing C/S ratio indicates an increasing number of S atoms bonded to OM

compounds in a sample matrix. The humic C/S ratio decreased with depth from 1.5 to 46.5 cm and from 2.6 to 45.5 cm in V1 and V2, respectively, suggesting potential sulfurization within the root and remineralization zone (Figure 1.15). Below 46 cm (burial zone) in V1 and V2, the C/S ratio relatively stabilized (decreased slightly) and values converged between 15 and 20. These observations are consistent with the idea of organic sulfur compounds forming within the root and remineralization zones of vegetated regions of the marsh and being selectively preserved in the burial zone relative to the rest of the OM pool over time as has been suggested to occur in a variety of sedimentary environments (Vairavamurthy et al., 1992; Sinninghe Damste and De Leeuw, 1990; Werne et al., 2000). Additionally, Ferdelman (1994) observed humic C/S ratios at the surface of the Great Marsh in September (closest sampling date to October in this dataset) and June of 1990 to be 57.4 and 78.9, respectively. Soils dated to 1990 in V1 and V2 were roughly 16.5 and 11.7 cm deep, respectively. The humic C/S ratio at these depths in V1 and V2 (Figure 1.15) were approximately 58.4 and 71.2, respectively. The humic C/S ratio in June surface soils in 1990 have either remained the same or dropped by 10%. A more detailed analysis such as Fourier transform ion cyclotron mass spectrometry (FTICR-MS) would be needed to verify these conclusions (similar to the approach used by Abdulla et al., 2020). HA C/S values in UV1 and UV2 remained relatively constant throughout the core and converged with V1 and V2 values at greater depths (ranging from 13-35 at ~80 cm). Humic C/N, Bulk soil S, and humic S depth profiles are shown in Figure Figure A6, respectively.

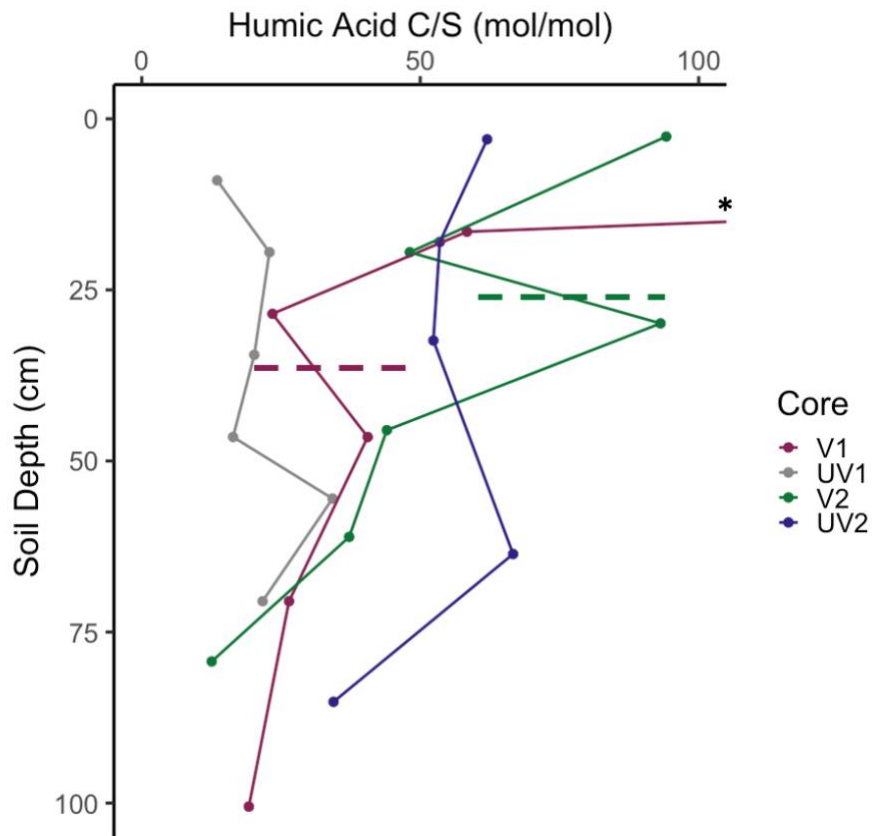


Figure 1.15: Humic acid C/S depth profile of cores collected in October 2020 and June 2021. Dashed lines indicate the bottom of the root zone in V1 (34.5 cm) and V2 (27.3 cm). *The V1 surface value (1.5 cm) was 538.2 mol/mol.

Sulfurization was only observed in the root zone of vegetated cores. This likely relates to redox chemistry in surface soils which is influenced by *S. alterniflora* biomass (Luther and Church, 1988; Koretsky et al., 2008). However, porewater HS- and Fe²⁺ (two major species affecting redox chemistry in salt marshes; Luther and Church 1988) profiles did not reveal vegetational trends (Figure 1.16 and Figure 1.17; found in a table format in Table A3 and Table A4). Although sulfide concentrations were higher in the surface soils of V2 than those of UV2, surface values were very

similar between V1 and UV1. The lack of differences in the June cores may reflect that the data acquired here represent only snapshots in time rather than a larger dataset, representative of the true biogeochemical environment experienced over longer, seasonal timescales. Seasonal differences, however, were found in these data.

Porewater HS^- concentrations were higher in June than October at both the surface and at most depths. HS^- values in V2 decreased from 4020 μM at 1.3 cm to ~ 550 μM at the bottom of the root zone (27.3 cm) while values in UV2 decreased from 1206 μM at 3.6 cm to ~ 825 μM at 27.3 cm. In the anoxic zone, almost all forms of solid iron (“reactive” Fe) react with S^{2-} to form FeS_2 (pyrite; Rickard and Luther, 2007). Once all the reactive Fe has reacted, sulfide concentrations increase and become available for sulfurization, as seen at depths below the root zone here. HS^- values increased at depths below the root zone in both V2 and UV2, an indication that all the reactive Fe had reacted, leaving HS^- free to accumulate. The limited Fe^{2+} data here (Figure 1.17, Table A4) support this conclusion. Fe^{2+} concentrations in the surface of V2 and UV2 reached 660 and 92 μM , respectively, decreased with depth, and reached undetectable levels at 27.3 cm. In V1 and UV1 however, HS^- concentrations were relatively low at the surface, remained about the same until 34.5 cm (bottom of the root zone in V1), and increased slightly at depths greater than the root zone in UV1 but remained the same in V1. Fe^{2+} concentrations were also relatively low at the surface in V1 and UV1.

High sulfide concentrations in salt marsh porewaters have been observed with concomitant, low Fe^{2+} concentrations or vice versa (Luther and Church, 1988; Boulegue et al., 1982; Koretsky et al., 2008). Fe^{2+} and HS^- coexisting in the same space and time, as observed in V2, conflicts with previous work and our understanding of Fe

and S redox biogeochemistry. Though there were relatively high Fe^{2+} and HS^- concentrations occurring at the same depths in UV2, the approximately 10:1 ratio of $\text{HS}^-:\text{Fe}^{2+}$ at the surface has been observed in other studies (Luther and Church 1988), while these lower 8:1 and 4:1 ratios as observed in the surface soils of V2 have not. In conclusion, the porewater redox chemistry observed here was not sufficient to explain trends in the HA C/S ratios, but the presence of HS^- indicates that sulfurization can occur.

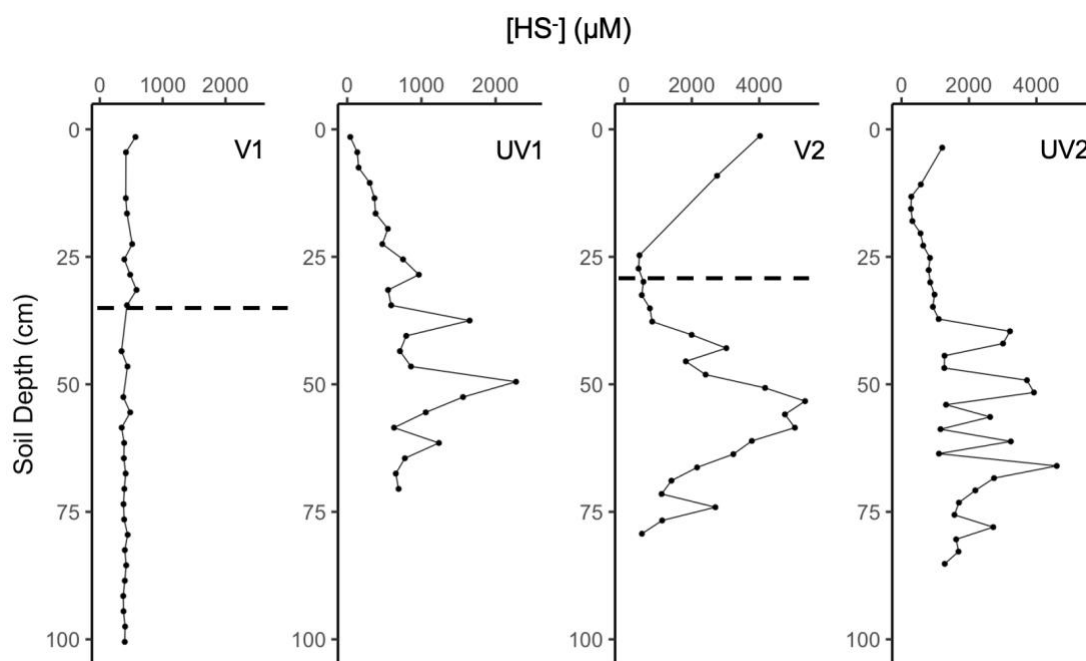


Figure 1.16: HS^- porewater concentrations over depth in cores collected in October 2020 and June 2021. Dashed lines indicate the bottom of the root zone in V1 (34.5 cm) and V2 (27.3 cm). Note that V1 and UV1 profiles have different x-axes than V2 and UV2 profiles.

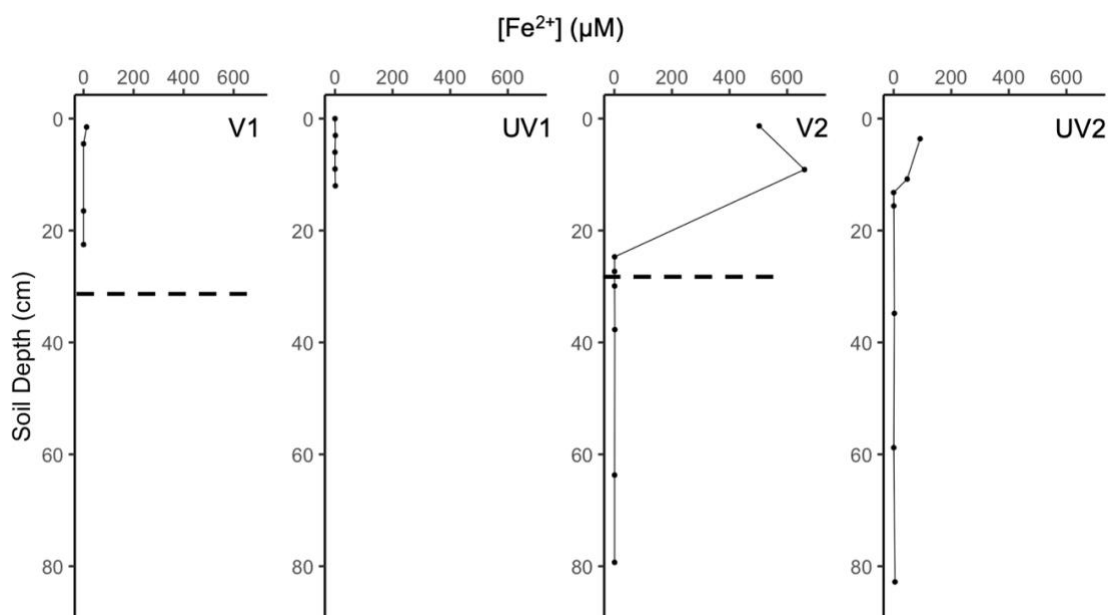


Figure 1.17: Fe^{2+} porewater concentrations over depth in cores collected in October 2020 and June 2021. Dashed lines indicate the bottom of the root zone in V1 (34.5 cm) and V2 (27.3 cm).

1.4 Concluding Remarks and Suggestions for Future Work

The amounts and composition of OM stored in salt marsh soils are important for understanding the formation of long-lived C pools and their value as blue carbon ecosystems. The OC accumulation rate of cores collected in this study varied with season (*S. alterniflora* phenophase), presence and lack of above-ground vegetation, and timescale. On average over a timescale of 144 ± 15 years, the OC accumulation rate of these cores was $65.7 \pm 13. \text{ g m}^{-2} \text{ yr}^{-1}$. This rate is much lower than regionally ($134.0 \pm 12.8 \text{ g m}^{-2} \text{ yr}^{-1}$) and globally ($244.7 \pm 26.1 \text{ g m}^{-2} \text{ yr}^{-1}$) reported rates, a result of roughly 50-year timescales being widely used by the blue C community to estimate OC burial rates. Shorter, decadal timescales generally mean shorter cores which contain a relatively higher percent of young, labile OC which result in inflated OC

inventories that ultimately inflate the estimated OC accumulation rate. Additionally, increasing rates of relative sea level rise over time increase sedimentation rates (Holmquist et al., 2021; Hill and Anisfield, 2015) which may add onto increasingly biased OC accumulation rate estimates over more recent timeframes. Since most studies collect short cores and use ^{137}Cs to date soils, regional and global averages tend to be inflated as well. Blue C ecosystems have been reported to bury OC approximately 50 times faster than temperate terrestrial forests (Mcleod et al., 2011). This observation has been used extensively to argue that salt marshes are more efficient than forests in removing CO_2 from the atmosphere (St. Laurent et al., 2020; Steinmuller et al., 2022; Li et al., 2022; Moritsch et al., 2022). However, terrestrial soil estimates are calculated over timescales of 700-15,000 years (Zehetner, 2010) while blue C estimates use timescales that only date back to 1963 and earlier. According to data compiled by Zehetner (2010), temperate terrestrial forest soils bury C at rates ranging from 14 to 58 $\text{g m}^{-2} \text{yr}^{-1}$ on an approximately 100-year timescale. On the same timescale, the Great Marsh buries C at rates ranging from 55.2 to 111.7 $\text{g m}^{-2} \text{yr}^{-1}$ (this study), values that turn out to be only 1-8 times those of terrestrial forests – and still represent a substantially shorter time of integration.

Given the factors that influence C accumulation rates, standardized procedures are needed so that data can be compared appropriately. Ultimately, the timing of core collection and the depth of integration for C accumulation rates should align with the research question. In the case of blue C and climate mitigation, C accumulation rates need to account not only for the C that is accumulating in the surface soils but also the C that is lost annually via remineralization and lateral transport processes below the root zone. Collecting soil cores that extend to at least 50 cm, or where soil OC

concentrations stabilize based on soil OC profiles, would effectively capture the quantitatively relevant C losses below the root zone, which avoids inflating accumulation rates. This approach requires no longer using ^{137}Cs as a dating tool and relying instead on ^{210}Pb and/or ^{14}C dating methods, depending on whether ^{210}Pb effectively dates soils to the net C balance depth. However, this approach could misconstrue OC dynamics over time with varying mineral levels that are dependent on marsh elevation (also variable). Additionally, longer timescales may not always be appropriate for the research question. For example, a study aiming to address salt marsh C burial rates over decadal changes in anthropogenic-induced sea level rise may require shorter timescales. Regardless, future studies that attempt to quantify the OC accumulation rate of a salt marsh should report the timescale used for accurate intercomparability and consider the higher relative accuracy that comes with longer cores/longer timescales. The blue C research community needs to recognize that currently reported global averages of salt marsh C burial rates are largely inflated estimates. All environments that bury OC offset anthropogenic CO_2 emissions and help mitigate climate change, but inaccurate overestimates of the role that salt marshes, and potentially other blue C environments, play in burying OC may be counterproductive.

Though OM characteristics in salt marsh soils are heterogeneous at the surface due to seasonal and vegetative influence, the data presented in this thesis suggest that they become increasingly homogenous with depth and diagenetic processing. Soil OC and porewater DOC concentrations as well as HA C/S ratios varied within the root zone in surface soils of the Great Marsh in both vegetated and unvegetated regions and throughout different times of the year. Surface soil OC concentrations, porewater

DOC concentrations, and HA C/S ratios were all higher in vegetated cores compared to unvegetated cores. Porewater DOC concentrations were higher in June than October. Values of all these parameters converged in the burial zone. Similarly, the distribution of C functional groups (as detected by ^{13}C NMR) became more similar with depth within the individual HA and bulk soil pools in all four cores. The distribution of C functional groups became more similar between HAs and bulk soils over depth as well. Diagenetic processes in the remineralization zone removed labile OC and transformed (and/or selectively preserved) OM in a way that increased its aromatic and decreased its O-alkyl, alkyl, and carboxyl character. It seems, therefore, that processes during early diagenesis in these salt marsh soils yield a more homogeneous OM pool as time progresses.

Processes that lead to OM preservation in soils and sediments include but are not limited to: 1) physical protection, 2) selective preservation (related to inherent recalcitrance), 3) humification 4) ecosystem properties, and 5) dilution (Hedges and Keil, 1995; Burdige, 2007; Zakem et al., 2021). The OM characteristics of the accumulating C in deep portions of our cores may thus reflect the OM that preferentially associates with minerals, or is inherently stable under the anoxic conditions in the Great Marsh soils. Consistent with previous work, the bulk soil OM became more similar in composition to HA and porewater FDOM showed higher degrees of humification over depth. The ^{13}C NMR data showed increasing aromatic abundance (a moiety often presumed to be inherently stable), while the elemental data show that the HA C/S ratio becomes much smaller, suggesting the potential preservation of sulfurized OM. The broad ^{13}C NMR signals also suggest Fe^{2+} and Fe^{3+} complexation with humic acids as a potential OM burial mechanism. High resolution

FTICR-MS analysis of bulk soils and HAs would provide more data for a detailed interpretation of the elemental transformations observed here with EA. This approach could, for example, detangle the results in the HA C/S ratios that hint at sulfurization being a driver of OC burial, corroborate whether CCAM content does in fact decrease with depth in HAs, and/or provide candidate compound classes for future investigations of mineral and interactions. Such analyses were planned for this thesis but have been delayed due to methodological issues and will be pursued with future work. $\delta^{13}\text{C}$ data could corroborate HA ^{13}C NMR results suggesting decreasing aquatic influence and increasing marsh soil influence with depth. Higher resolution HA depth profiles would allow for more precise interpretations leading to improved theories. Future work should be aimed at quantifying soil OC, calculating OC accumulation rates, and identifying OM trends over depth in cores collected during Dormancy and Maturity. Such analyses would fill the knowledge gaps in this study, providing a complete picture of seasonal soil C cycling in the Great Marsh. Collecting and analyzing soils during each phenophase over multiple years would further corroborate these results.

This thesis adds to the ever-growing volume of research dedicated to blue C cycling and soil OM properties. The timescale considerations presented here are important for accurately assessing the role that salt marshes play in C sequestration and global C cycling. More research and wetland monitoring that take these suggestions into consideration are needed to improve our understanding and management practices of blue C environments. Pinpointing the mechanisms driving C sequestration will improve our ability to identify high priority regions for conservation and restoration. Without care, these C sinks could soon become CO_2 sources.

Understanding the true impact that blue C environments have on offsetting worldwide anthropogenic climate change is urgent given that the global atmospheric CO₂ rate of increase and sea levels continue to rise which threaten the physical and chemical stability of salt marshes.

REFERENCES

- Abdulla, H. A., Burdige, D. J., & Komada, T. (2020). Abiotic formation of dissolved organic sulfur in anoxic sediments of Santa Barbara Basin. *Organic Geochemistry*, 139, 103879. <https://doi.org/10.1016/j.orggeochem.2019.05.009>
- Adani, F., Genevini, P., Tambone, F., & Montoneri, E. (2006). Compost effect on soil humic acid: A NMR study. *Chemosphere*, 65(8), 1414–1418. <https://doi.org/10.1016/j.chemosphere.2006.03.070>
- Bianchi, T.S. & Canuel, E.A. (2011). Lipids: Hydrocarbons. *Chemical biomarkers in aquatic ecosystems* (pp. 185-206). Princeton University Press. <https://doi.org/10.1515/9781400839100>
- Bianchi, T.S., Morrison, E., Barry, S., Arellano, A.R., Feagin, R.A., Hinson, A., Eriksson, M., Allison, M., Osburn, C.L., & Oviedo-Vargas, D. (2018). Chapter 4: The fate and transport of allochthonous blue carbon in divergent coastal systems. In L. Windham-Myers, *A blue carbon primer: the state of coastal wetland carbon science, practice and policy* (pp. 27-49). Taylor & Francis Group.
- Boulegue, J., Lord, C. J., & Church, T. M. (1982). Sulfur speciation and associated trace metals (Fe, Cu) in the pore waters of Great Marsh, Delaware. *Geochimica et Cosmochimica Acta*, 46(3), 453–464. [https://doi.org/10.1016/0016-7037\(82\)90236-8](https://doi.org/10.1016/0016-7037(82)90236-8)
- Brown, L. A., Dash, J., Ogutu, B. O., & Richardson, A. D. (2017). On the relationship between continuous measures of canopy greenness derived using near-surface remote sensing and satellite-derived vegetation products. *Agricultural and Forest Meteorology*, 247, 280–292. <https://doi.org/10.1016/j.agrformet.2017.08.012>
- Burdige, D. J. (2007). Preservation of Organic Matter in Marine Sediments: Controls, Mechanisms, and an Imbalance in Sediment Organic Carbon Budgets? *Chemical Reviews*, 107(2), 467–485. <https://doi.org/10.1021/cr050347q>
- Carr, S. J., Diggins, L. M., & Spencer, K. L. (2020). There is no such thing as ‘undisturbed’ soil and sediment sampling: Sampler-induced deformation of salt marsh sediments revealed by 3D X-ray computed tomography. *Journal of Soils and Sediments*, 20(7), 2960–2976. <https://doi.org/10.1007/s11368-020-02655-7>

- Champlin, Velinsky, Tucker, Sommerfield, Laurent, & Watson. (2020). Carbon Sequestration Rate Estimates in Delaware Bay and Barnegat Bay Tidal Wetlands Using Interpolation Mapping. *Data*, 5(1), 11. <https://doi.org/10.3390/data5010011>
- Chen, X., Jin, M., Xu, Y., Chu, W., Olk, D. C., Hu, J., Jiang, Y., Mao, J., Gao, H., & Thompson, M. L. (2019). Potential Alterations in the Chemical Structure of Soil Organic Matter Components during Sodium Hydroxide Extraction. *Journal of Environmental Quality*, 48(6), 1578–1586. <https://doi.org/10.2134/jeq2019.02.0077>
- Chmura, G. L. (2013). What do we need to assess the sustainability of the tidal salt marsh carbon sink? *Ocean & Coastal Management*, 83, 25–31. <https://doi.org/10.1016/j.ocecoaman.2011.09.006>
- Chmura, G. L., Anisfeld, S. C., Cahoon, D. R., & Lynch, J. C. (2003). Global carbon sequestration in tidal, saline wetland soils. *Global Biogeochemical Cycles*, 17(4). <https://doi.org/10.1029/2002GB001917>
- Corcoran, M., Sherif, M. I., Smalley, C., Li, A., Rockne, K. J., Giesy, J. P., & Sturchio, N. C. (2018). Accumulation rates, focusing factors, and chronologies from depth profiles of ²¹⁰Pb and ¹³⁷Cs in sediments of the Laurentian Great Lakes. *Journal of Great Lakes Research*, 44(4), 693–704. <https://doi.org/10.1016/j.jglr.2018.05.013>
- Crooks, S., Sutton-Grier, A. E., Troxler, T. G., Herold, N., Bernal, B., Schile-Beers, L., & Wirth, T. (2018). Coastal wetland management as a contribution to the US National Greenhouse Gas Inventory. *Nature Climate Change*, 8(12), 1109–1112. <https://doi.org/10.1038/s41558-018-0345-0>
- Daiber, F. C. (1974). Salt marsh plants and future coastal salt marshes in relation to animals. In *Ecology of Halophytes* (pp. 475–508). Elsevier. <https://doi.org/10.1016/B978-0-12-586450-3.50021-4>
- DeFranco, K. C., Ricketts, M. P., Blanc-Betes, E., Welker, J. M., Gonzalez-Meler, M. A., & Sturchio, N. C. (2020). Deeper snow increases the net soil organic carbon accrual rate in moist acidic tussock tundra: ²¹⁰Pb evidence from Arctic Alaska. *Arctic, Antarctic, and Alpine Research*, 52(1), 461–475. <https://doi.org/10.1080/15230430.2020.1802864>
- DeLaune, R. D., White, J. R., Elsey-Quirk, T., Roberts, H. H., & Wang, D. Q. (2018). Differences in long-term vs short-term carbon and nitrogen sequestration in a coastal river delta wetland: Implications for global budgets. *Organic Geochemistry*, 123, 67–73. <https://doi.org/10.1016/j.orggeochem.2018.06.007>

- DiDonato, N., Chen, H., Waggoner, D., & Hatcher, P. G. (2016). Potential origin and formation for molecular components of humic acids in soils. *Geochimica et Cosmochimica Acta*, 178, 210–222. <https://doi.org/10.1016/j.gca.2016.01.013>
- Drexler, J. Z., Fuller, C. C., Orlando, J., Salas, A., Wurster, F. C., & Duberstein, J. A. (2017). Estimation and Uncertainty of Recent Carbon Accumulation and Vertical Accretion in Drained and Undrained Forested Peatlands of the Southeastern USA: Drained and Intact Forested Peatlands. *Journal of Geophysical Research: Biogeosciences*, 122(10), 2563–2579. <https://doi.org/10.1002/2017JG003950>
- Drexler, J. Z., Fuller, C. C., & Archfield, S. (2018). The approaching obsolescence of ¹³⁷Cs dating of wetland soils in North America. *Quaternary Science Reviews*, 199, 83–96. <https://doi.org/10.1016/j.quascirev.2018.08.028>
- Duarte, C. M., Middelburg, J. J., & Caraco, N. (2005). *Major role of marine vegetation on the oceanic carbon cycle*. 8.
- Ellis, A. J., & Golding, R. M. (1959). 25. Spectrophotometric determination of the acid dissociation constants of hydrogen sulphide. *J. Chem. Soc.*, 0, 127–130. <https://doi.org/10.1039/JR9590000127>
- Enríquez, S., Duarte, C. M., & Sand-Jensen, K. (1993). Patterns in decomposition rates among photosynthetic organisms: The importance of detritus C:N:P content. *Oecologia*, 94(4), 457–471. <https://doi.org/10.1007/BF00566960>
- Ferdelman, T.G. (1994). *Oceanographic and geochemical controls on sulfur diagenesis in coastal sediments* [Doctoral dissertation, University of Delaware].
- Ferdelman, T. G., Church, T. M., & Luther, G. W. (1991). Sulfur enrichment of humic substances in a Delaware salt marsh sediment core. *Geochimica et Cosmochimica Acta*, 55(4), 979–988. [https://doi.org/10.1016/0016-7037\(91\)90156-Y](https://doi.org/10.1016/0016-7037(91)90156-Y)
- Filip, Z., Alberts, J. J., Cheshire, M. V., Goodman, B. A., & Bacon, J. R. (1988). Comparison of salt marsh humic acid with humic-like substances from the indigenous plant species *Spartina alterniflora* (Loisel). *Science of The Total Environment*, 71(2), 157–172.
- Friedrichs, C. T., & Perry, J. E. (2021). *Tidal Salt Marsh Morphodynamics: A Synthesis*. 32.

- Grannas, A. M., Cory, R. M., Miller, P. L., Chin, Y.-P., & McKnight, D. M. (2012). The role of dissolved organic matter in arctic surface waters in the photolysis of hexachlorobenzene and lindane: DOM-MEDIATED PHOTOLYSIS OF POPs. *Journal of Geophysical Research: Biogeosciences*, 117(G1). <https://doi.org/10.1029/2010JG001518>
- Gomez-Saez, G. V., Niggemann, J., Dittmar, T., Pohlabein, A. M., Lang, S. Q., Noowong, A., Pichler, T., Wörmer, L., & Bühring, S. I. (2016). Molecular evidence for abiotic sulfurization of dissolved organic matter in marine shallow hydrothermal systems. *Geochimica et Cosmochimica Acta*, 190, 35–52. <https://doi.org/10.1016/j.gca.2016.06.027>
- Hatcher, P. G., Spiker, E. C., Szeverenyi, N. M., & Maciel, G. E. (1983). Selective preservation and origin of petroleum-forming aquatic kerogen. *Nature*, 305(5934), 498–501. <https://doi.org/10.1038/305498a0>
- Hedges, J. I., & Keil, R. G. (1995). Sedimentary organic matter preservation: An assessment and speculative synthesis. *Marine Chemistry*, 36.
- Henneke, E., Luther, G. W., De Lange, G. J., & Hoefs, J. (1997). Sulphur speciation in anoxic hypersaline sediments from the eastern Mediterranean Sea. *Geochimica et Cosmochimica Acta*, 61(2), 307–321. [https://doi.org/10.1016/S0016-7037\(96\)00355-9](https://doi.org/10.1016/S0016-7037(96)00355-9)
- Hill, T. D., & Anisfeld, S. C. (2015). Coastal wetland response to sea level rise in Connecticut and New York. *Estuarine, Coastal and Shelf Science*, 163, 185–193. <https://doi.org/10.1016/j.ecss.2015.06.004>
- Holmquist, J. R., Windham-Myers, L., Bernal, B., Byrd, K. B., Crooks, S., Gonnee, M. E., Herold, N., Knox, S. H., Kroeger, K. D., McCombs, J., Megonigal, J. P., Lu, M., Morris, J. T., Sutton-Grier, A. E., Troxler, T. G., & Weller, D. E. (2018). Uncertainty in United States coastal wetland greenhouse gas inventorying. *Environmental Research Letters*, 13(11), 115005. <https://doi.org/10.1088/1748-9326/aae157>
- Holmquist, J. R., Brown, L. N., & MacDonald, G. M. (2021). Localized Scenarios and Latitudinal Patterns of Vertical and Lateral Resilience of Tidal Marshes to Sea-Level Rise in the Contiguous United States. *Earth's Future*, 9(6). <https://doi.org/10.1029/2020EF001804>
- Johnson, R. L., & Schmidt-Rohr, K. (2014). Quantitative solid-state ¹³C NMR with signal enhancement by multiple cross polarization. *Journal of Magnetic Resonance*, 239, 44–49. <https://doi.org/10.1016/j.jmr.2013.11.009>

- Kaiser, K., & Guggenberger, G. (2000). The role of DOM sorption to mineral surfaces in the preservation of organic matter in soils. *Organic Geochemistry*, 31(7–8), 711–725. [https://doi.org/10.1016/S0146-6380\(00\)00046-2](https://doi.org/10.1016/S0146-6380(00)00046-2)
- Kayranli, B., Scholz, M., Mustafa, A., & Hedmark, Å. (2010). Carbon Storage and Fluxes within Freshwater Wetlands: A Critical Review. *Wetlands*, 30(1), 111–124. <https://doi.org/10.1007/s13157-009-0003-4>
- Kelleway, J. J., Saintilan, N., Macreadie, P. I., Baldock, J. A., Heijnis, H., Zawadzki, A., Gadd, P., Jacobsen, G., & Ralph, P. J. (2017). Geochemical analyses reveal the importance of environmental history for blue carbon sequestration. *Journal of Geophysical Research: Biogeosciences*, 122(7), 1789–1805. <https://doi.org/10.1002/2017JG003775>
- Kleber, M., & Lehmann, J. (2019). Humic Substances Extracted by Alkali Are Invalid Proxies for the Dynamics and Functions of Organic Matter in Terrestrial and Aquatic Ecosystems. *Journal of Environmental Quality*, 48(2), 207–216. <https://doi.org/10.2134/jeq2019.01.0036>
- Koretsky, C. M., Haveman, M., Cuellar, A., Beuving, L., Shattuck, T., & Wagner, M. (2008). Influence of *Spartina* and *Juncus* on Saltmarsh Sediments. I. Pore Water Geochemistry. *Chemical Geology*, 255(1–2), 87–99. <https://doi.org/10.1016/j.chemgeo.2008.06.013>
- Kuzyakov, Y. (2014). Biochar stability in soil: Decomposition during eight years and transformation as assessed by compound-specific ¹⁴C analysis. *Soil Biology*, 8.
- Lamar, R. T., Olk, D. C., Mayhew, L., & Bloom, P. R. (2014). A New Standardized Method for Quantification of Humic and Fulvic Acids in Humic Ores and Commercial Products. *Journal of AOAC INTERNATIONAL*, 97(3), 721–730. <https://doi.org/10.5740/jaoacint.13-393>
- Lee, C. (1992). Controls on organic carbon preservation: The use of stratified water bodies to compare intrinsic rates of decomposition in oxic and anoxic systems. *Geochimica et Cosmochimica Acta*, 56(8), 3323–3335. [https://doi.org/10.1016/0016-7037\(92\)90308-6](https://doi.org/10.1016/0016-7037(92)90308-6)
- Lehmann, J., & Kleber, M. (2015). The contentious nature of soil organic matter. *Nature*, 528(7580), 60–68. <https://doi.org/10.1038/nature16069>

- Li, J., Yan, D., Yao, X., Liu, Y., Xie, S., Sheng, Y., & Luan, Z. (2022). Dynamics of Carbon Storage in Saltmarshes Across China's Eastern Coastal Wetlands From 1987 to 2020. *Frontiers in Marine Science*, 9, 915727. <https://doi.org/10.3389/fmars.2022.915727>
- Liu, J., Shu, Z., Zhao, Y., Deng, D., Zou, C., Xin, Y., & Zhang, L. (2021). Changes in the chemical composition of the organic carbon in *Spartina alterniflora* litter during decomposition in saltmarsh sediments. *Journal of Soils and Sediments*, 21(10), 3438–3450. <https://doi.org/10.1007/s11368-021-02975-2>
- Loomis, M. J., & Craft, C. B. (2010). Carbon Sequestration and Nutrient (Nitrogen, Phosphorus) Accumulation in River-Dominated Tidal Marshes, Georgia, USA. *Soil Science Society of America Journal*, 74(3), 1028–1036. <https://doi.org/10.2136/sssaj2009.0171>
- Luther, G. W., & Church, T. M. (1988). Seasonal cycling of sulfur and iron in porewaters of a Delaware salt marsh. *Marine Chemistry*, 23(3–4), 295–309. [https://doi.org/10.1016/0304-4203\(88\)90100-4](https://doi.org/10.1016/0304-4203(88)90100-4)
- Luther, G. W., Findlay, A. J., MacDonald, D. J., Owings, S. M., Hanson, T. E., Beinart, R. A., & Girguis, P. R. (2011). Thermodynamics and Kinetics of Sulfide Oxidation by Oxygen: A Look at Inorganically Controlled Reactions and Biologically Mediated Processes in the Environment. *Frontiers in Microbiology*, 2. <https://doi.org/10.3389/fmicb.2011.00062>
- Mao, J.-D., Hu, W.-G., Schmidt-Rohr, K., Davies, G., Ghabbour, E. A., & Xing, B. (2000). Quantitative Characterization of Humic Substances by Solid-State Carbon-13 Nuclear Magnetic Resonance. *Soil Science Society of America Journal*, 64(3), 873–884. <https://doi.org/10.2136/sssaj2000.643873x>
- Mao, J.-D., Tremblay, L., Gagné, J.-P., Kohl, S., Rice, J., & Schmidt-Rohr, K. (2007). Humic acids from particulate organic matter in the Saguenay Fjord and the St. Lawrence Estuary investigated by advanced solid-state NMR. *Geochimica et Cosmochimica Acta*, 71(22), 5483–5499. <https://doi.org/10.1016/j.gca.2007.09.022>
- Mcleod, E., Chmura, G. L., Bouillon, S., Salm, R., Björk, M., Duarte, C. M., Lovelock, C. E., Schlesinger, W. H., & Silliman, B. R. (2011). A blueprint for blue carbon: Toward an improved understanding of the role of vegetated coastal habitats in sequestering CO₂. *Frontiers in Ecology and the Environment*, 9(10), 552–560. <https://doi.org/10.1890/110004>

- Millero, F. J., Hubinger, Scott., Fernandez, Marino., & Garnett, Stephen. (1987). Oxidation of H₂S in seawater as a function of temperature, pH, and ionic strength. *Environmental Science & Technology*, 21(5), 439–443. <https://doi.org/10.1021/es00159a003>
- Moritsch, M. M., Byrd, K. B., Davis, M., Good, A., Drexler, J. Z., Morris, J. T., Woo, I., Windham-Myers, L., Grossman, E., Nakai, G., Poppe, K. L., & Rybczyk, J. M. (2022). Can Coastal Habitats Rise to the Challenge? Resilience of Estuarine Habitats, Carbon Accumulation, and Economic Value to Sea-Level Rise in a Puget Sound Estuary. *Estuaries and Coasts*. <https://doi.org/10.1007/s12237-022-01087-5>
- Morris, J.T. & Callaway, J.C. (2018). Chapter 6: Physical and biological regulation of carbon sequestration in tidal marshes. In L.Windham-Myers, *A blue carbon primer: the state of coastal wetland carbon science, practice and policy* (pp. 67-79). Taylor & Francis Group.
- Mueller, P., Ladiges, N., Jack, A., Schmiedl, G., Kutzbach, L., Jensen, K., & Nolte, S. (2019). Assessing the long-term carbon-sequestration potential of the semi-natural salt marshes in the European Wadden Sea. *Ecosphere*, 10(1). <https://doi.org/10.1002/ecs2.2556>
- Najjar, R. G., Herrmann, M., Alexander, R., Boyer, E. W., Burdige, D. J., Butman, D., Cai, W. -J., Canuel, E. A., Chen, R. F., Friedrichs, M. A. M., Feagin, R. A., Griffith, P. C., Hinson, A. L., Holmquist, J. R., Hu, X., Kemp, W. M., Kroeger, K. D., Mannino, A., McCallister, S. L., ... Zimmerman, R. C. (2018). Carbon Budget of Tidal Wetlands, Estuaries, and Shelf Waters of Eastern North America. *Global Biogeochemical Cycles*, 32(3), 389–416. <https://doi.org/10.1002/2017GB005790>
- National Oceanic and Atmospheric Administration (NOAA). (2009). *Sea level variations of the United States 1854-2006* (Technical Report No. NOS CO-OPS 053). https://tidesandcurrents.noaa.gov/publications/Tech_rpt_53.pdf
- Nellemann, C., Corcoran, E., Duarte, C. M., Valdés, L., De Young, C., Fonseca, L., Grimsditch, G. (Eds). 2009. Blue Carbon. A Rapid Response Assessment. United Nations Environment Programme, GRID-Arendal, www.grida.no
- Nyman, J. A., Walters, R. J., Delaune, R. D., & Patrick, W. H. (2006). Marsh vertical accretion via vegetative growth. *Estuarine, Coastal and Shelf Science*, 69(3–4), 370–380. <https://doi.org/10.1016/j.ecss.2006.05.041>

- Ohno, T. (2002). Fluorescence Inner-Filtering Correction for Determining the Humification Index of Dissolved Organic Matter. *Environmental Science & Technology*, 36(4), 742–746. <https://doi.org/10.1021/es0155276>
- Olk, D. C., Bloom, P. R., Perdue, E. M., McKnight, D. M., Chen, Y., Fahrenhorst, A., Senesi, N., Chin, Y.-P., Schmitt-Kopplin, P., Hertkorn, N., & Harir, M. (2019). Environmental and Agricultural Relevance of Humic Fractions Extracted by Alkali from Soils and Natural Waters. *Journal of Environmental Quality*, 48(2), 217–232. <https://doi.org/10.2134/jeq2019.02.0041>
- Ouyang, X., & Lee, S. Y. (2014). Updated estimates of carbon accumulation rates in coastal marsh sediments. *Biogeosciences*, 11(18), 5057–5071. <https://doi.org/10.5194/bg-11-5057-2014>
- Petit, J. R., Jouzel, J., Raynaud, D., Barkov, N. I., Delaygue, G., Delmotte, M., Kotlyakov, V. M., Legrand, M., Lipenkov, V. Y., Lorius, C., & Saltzman, E. (1999). *Climate and atmospheric history of the past 420,000 years from the Vostok ice core, Antarctica*. 399, 8.
- Pohlabein, A. M., Gomez-Saez, G. V., Noriega-Ortega, B. E., & Dittmar, T. (2017). Experimental Evidence for Abiotic Sulfurization of Marine Dissolved Organic Matter. *Frontiers in Marine Science*, 4, 364. <https://doi.org/10.3389/fmars.2017.00364>
- Raven, M. R., Sessions, A. L., Adkins, J. F., & Thunell, R. C. (2016). Rapid organic matter sulfurization in sinking particles from the Cariaco Basin water column. *Geochimica et Cosmochimica Acta*, 190, 175–190. <https://doi.org/10.1016/j.gca.2016.06.030>
- Roman, C., & Daiber, F. (1989). Organic carbon flux through a Delaware Bay salt marsh: Tidal exchange, particle size distribution, and storms. *Marine Ecology Progress Series*, 54, 149–156. <https://doi.org/10.3354/meps054149>
- Sadler, P. M. (1999). *Determination of Sediment Accumulation Rates*. 5, 26.
- Santín, C., González-Pérez, M., Otero, X. L., Vidal-Torrado, P., Macías, F., & Álvarez, M. Á. (2008). Characterization of humic substances in salt marsh soils under sea rush (*Juncus maritimus*). *Estuarine, Coastal and Shelf Science*, 79(3), 541–548. <https://doi.org/10.1016/j.ecss.2008.05.007>
- Schelske, C.L. & Odum, E.P. (1962). *Mechanisms maintaining high productivity in Georgia estuaries* [Paper presentation]. Proceedings of the Gulf and Caribbean Fisheries Institute, 14. <http://hdl.handle.net/1834/28220>

- Schiebel, H. N., Gardner, G. B., Wang, X., Peri, F., & Chen, R. F. (2018). Seasonal Export of Dissolved Organic Matter from a New England Salt Marsh. *Journal of Coastal Research*, 344, 939–954. <https://doi.org/10.2112/JCOASTRES-D-16-00196.1>
- Seyfferth, A. L., Bothfeld, F., Vargas, R., Stuckey, J. W., Wang, J., Kearns, K., Michael, H. A., Guimond, J., Yu, X., & Sparks, D. L. (2020). Spatial and temporal heterogeneity of geochemical controls on carbon cycling in a tidal salt marsh. *Geochimica et Cosmochimica Acta*, 282, 1–18. <https://doi.org/10.1016/j.gca.2020.05.013>
- Sinninghe Damste, J. S., & De Leeuw, J. W. (1990). Analysis, structure and geochemical significance of organically-bound sulphur in the geosphere: State of the art and future research. *Organic Geochemistry*, 16(4–6), 1077–1101. [https://doi.org/10.1016/0146-6380\(90\)90145-P](https://doi.org/10.1016/0146-6380(90)90145-P)
- Spencer, R.G.M. & Coble P.G. (2014). Chapter 4: Sampling design for organic matter fluorescence analysis. In P.G. Coble, J. Lead, A. Baker, D.M. Reynolds, & R.G.M. Spencer, *Aquatic Organic Matter Fluorescence* (pp. 125-146). Cambridge University Press.
- Steinmuller, H. E., Breithaupt, J. L., Engelbert, K. M., Assavapanuvat, P., & Bianchi, T. S. (2022). Coastal Wetland Soil Carbon Storage at Mangrove Range Limits in Apalachicola Bay, FL: Observations and Expectations. *Frontiers in Forests and Global Change*, 5, 852910. <https://doi.org/10.3389/ffgc.2022.852910>
- Stevenson, F.J. (1994). *Humus chemistry: genesis, composition, reactions*. John Wiley & Sons.
- St. Laurent, K. A., Hribar, D. J., Carlson, A. J., Crawford, C. M., & Siok, D. (2020). Assessing coastal carbon variability in two Delaware tidal marshes. *Journal of Coastal Conservation*, 24(6), 65. <https://doi.org/10.1007/s11852-020-00783-3>
- Stookey, L. L. (1970). Ferrozine—A new spectrophotometric reagent for iron. *Analytical Chemistry*, 42(7), 779–781. <https://doi.org/10.1021/ac60289a016>
- Stumpf, R.P. (1983). The process of sedimentation on the surface of a salt marsh. *Estuarine, Coastal, and Shelf Science*, 17, 495-508.
- Sun, H., Jiang, J., Cui, L., Feng, W., Wang, Y., & Zhang, J. (2019). Soil organic carbon stabilization mechanisms in a subtropical mangrove and salt marsh ecosystems. *Science of The Total Environment*, 673, 502–510. <https://doi.org/10.1016/j.scitotenv.2019.04.122>

- Thorn, K.A., Folan, D.W., & MacCarthy, P. (1989). *Characterization of the International Humic Substances Society Standard and Reference Fulvic and Humic Acids by Solution State Carbon-13 (¹³C) and Hydrogen-1 (¹H) Nuclear Magnetic Resonance Spectrometry* (Water-Resources Investigations Report No. 89-4196). United States Geological Survey. <https://pubs.usgs.gov/wri/1989/4196/report.pdf>
- Tissot, B.P. & Welte, D.H. (1984). Diagenesis, Catagenesis and Metagenesis of Organic Matter. In: *Petroleum Formation and Occurrence*. Springer, Berlin, Heidelberg. https://doi.org/10.1007/978-3-642-87813-8_6
- Tobias, C. & Neubauer, S.C. (2019). Chapter 16: Salt marsh biogeochemistry – an overview. In G.M.E. Perillo, E. Wolanski, D.R. Cahoon, & M.M. Brinson. *Coastal wetlands: An integrated ecological approach* (pp. 539-577). Elsevier. <https://doi.org/10.1016/B978-0-444-63893-9.00016-2>
- Tucker, K.J. (2016). *Variability of organic carbon accumulation on a tidal wetland coast* [Doctoral dissertation, University of Delaware]. UDSpace. <http://udspace.udel.edu/handle/19716/17729>
- Unger, V., Elsey-Quirk, T., Sommerfield, C., & Velinsky, D. (2016). Stability of organic carbon accumulating in *Spartina alterniflora*-dominated salt marshes of the Mid-Atlantic U.S. *Estuarine, Coastal and Shelf Science*, 182, 179–189. <https://doi.org/10.1016/j.ecss.2016.10.001>
- Vairavamurthy, A., Mopper, K., & Taylor, B. F. (1992). Occurrence of particle-bound polysulfides and significance of their reaction with organic matters in marine sediments. *Geophysical Research Letters*, 19(20), 2043–2046. <https://doi.org/10.1029/92GL01995>
- Van de Broek, M., Temmerman, S., Merckx, R., & Govers, G. (2016). Controls on soil organic carbon stocks in tidal marshes along an estuarine salinity gradient. *Biogeosciences*, 13(24), 6611–6624. <https://doi.org/10.5194/bg-13-6611-2016>
- Vázquez-Lule, A., & Vargas, R. (2021). Biophysical drivers of net ecosystem and methane exchange across phenological phases in a tidal salt marsh. *Agricultural and Forest Meteorology*, 300, 108309. <https://doi.org/10.1016/j.agrformet.2020.108309>
- Wallbrink, P.J., Walling, D.E., and He, Q. (2002). Radionuclide measurement using HPGe gamma spectrometry. In: Zapata, F., ed. *Handbook for the assessment of soil erosion and sedimentation using environmental radionuclides*. Kluwer Academic Publisher, pp. 67-96. https://www-pub.iaea.org/MTCD/Publications/PDF/TE-1741_web.pdf

- Werne, J. P., Hollander, D. J., Behrens, A., Schaeffer, P., Albrecht, P., & Sinninghe Damsté, J. S. (2000). Timing of early diagenetic sulfurization of organic matter: A precursor-product relationship in Holocene sediments of the anoxic Cariaco Basin, Venezuela. *Geochimica et Cosmochimica Acta*, 64(10), 1741–1751. [https://doi.org/10.1016/S0016-7037\(99\)00366-X](https://doi.org/10.1016/S0016-7037(99)00366-X)
- Witte, E. G., Philipp, H., & Vereecken, H. (1998). Binding of ¹³C-labelled 2-aminobenzothiazoles to humic acid as derived from ¹³C NMR spectroscopy. *Organic Geochemistry*, 29(5–7), 1829–1835. [https://doi.org/10.1016/S0146-6380\(98\)00074-6](https://doi.org/10.1016/S0146-6380(98)00074-6)
- Wozniak, A. S., Goranov, A. I., Mitra, S., Bostick, K. W., Zimmerman, A. R., Schlesinger, D. R., Myneni, S., & Hatcher, P. G. (2020). Molecular heterogeneity in pyrogenic dissolved organic matter from a thermal series of oak and grass chars. *Organic Geochemistry*, 148, 104065. <https://doi.org/10.1016/j.orggeochem.2020.104065>
- Yücel, M., Konovalov, S. K., Moore, T. S., Janzen, C. P., & Luther, G. W. (2010). Sulfur speciation in the upper Black Sea sediments. *Chemical Geology*, 269(3–4), 364–375. <https://doi.org/10.1016/j.chemgeo.2009.10.010>
- Yuknis, N. L. (2012). *Soil Accretion and Organic Carbon Accumulation in the Tidal Salt Marshes of the Liaohe Delta, China*. [Master's thesis, Louisiana State University]. LSU Digital Commons. https://digitalcommons.lsu.edu/gradschool_theses/425
- Zakem, E. J., Cael, B. B., & Levine, N. M. (2021). A unified theory for organic matter accumulation. *Proceedings of the National Academy of Sciences*, 118(6), e2016896118. <https://doi.org/10.1073/pnas.2016896118>
- Zech, W., Senesi, N., Guggenberger, G., Kaiser, K., Lehmann, J., Miano, T. M., Miltner, A., & Schroth, G. (1997). Factors controlling humification and mineralization of soil organic matter in the tropics. *Geoderma*, 79(1–4), 117–161. [https://doi.org/10.1016/S0016-7061\(97\)00040-2](https://doi.org/10.1016/S0016-7061(97)00040-2)
- Zehetner, F. (2010). Does organic carbon sequestration in volcanic soils offset volcanic CO₂ emissions? *Quaternary Science Reviews*, 29(11–12), 1313–1316. <https://doi.org/10.1016/j.quascirev.2010.03.003>
- Zhao, Q., Bai, J., Liu, Q., Lu, Q., Gao, Z., & Wang, J. (2016). Spatial and Seasonal Variations of Soil Carbon and Nitrogen Content and Stock in a Tidal Salt Marsh with *Tamarix chinensis*, China. *Wetlands*, 36(S1), 145–152. <https://doi.org/10.1007/s13157-015-0647-1>

Appendix

FIGURES

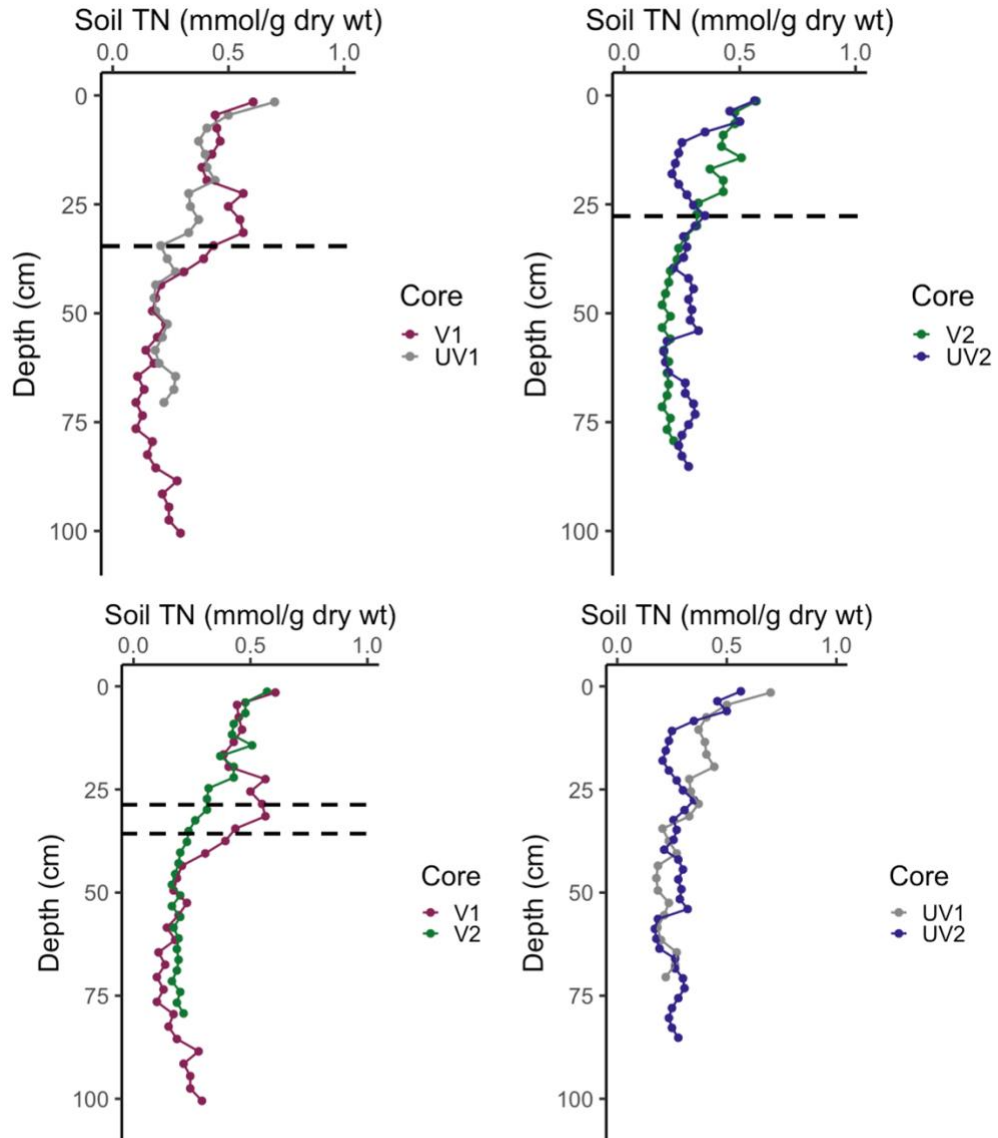


Figure A1: Soil TN depth profiles of vegetated (left) and unvegetated (right) cores to highlight vegetative (top) and seasonal (bottom) differences. Dashed lines indicate the bottom of the root zone in V1 (34.5 cm) and V2 (27.3 cm).

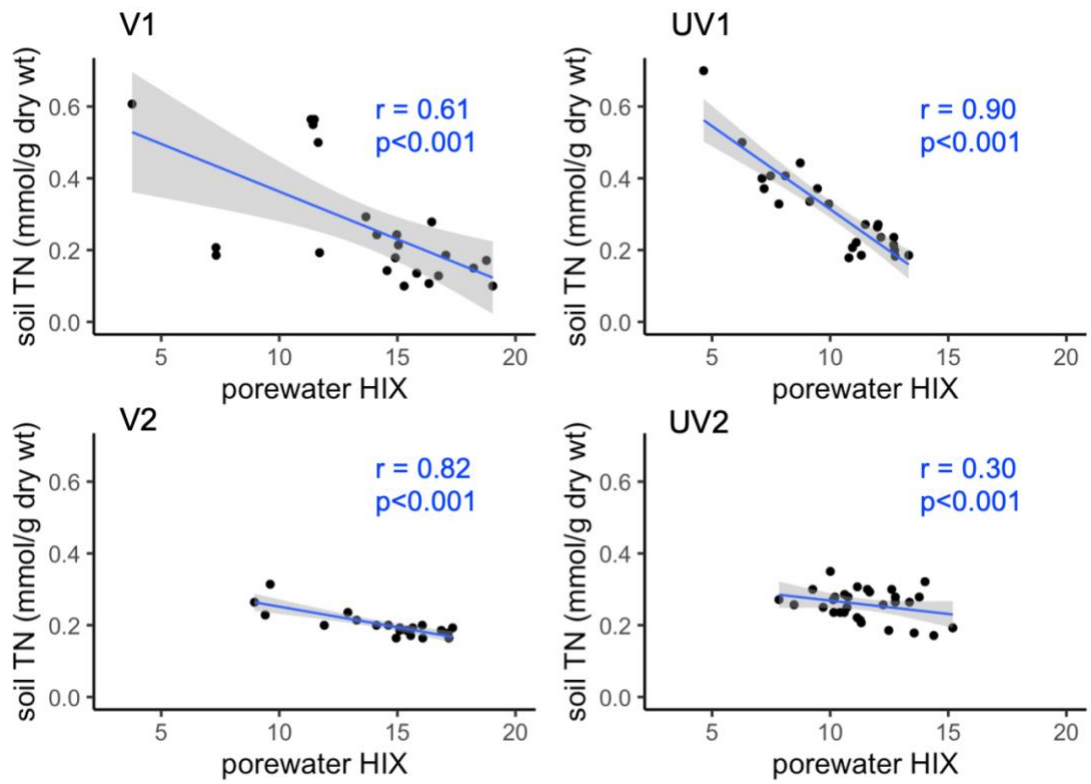


Figure A2: Correlation between soil TN and porewater HIX.

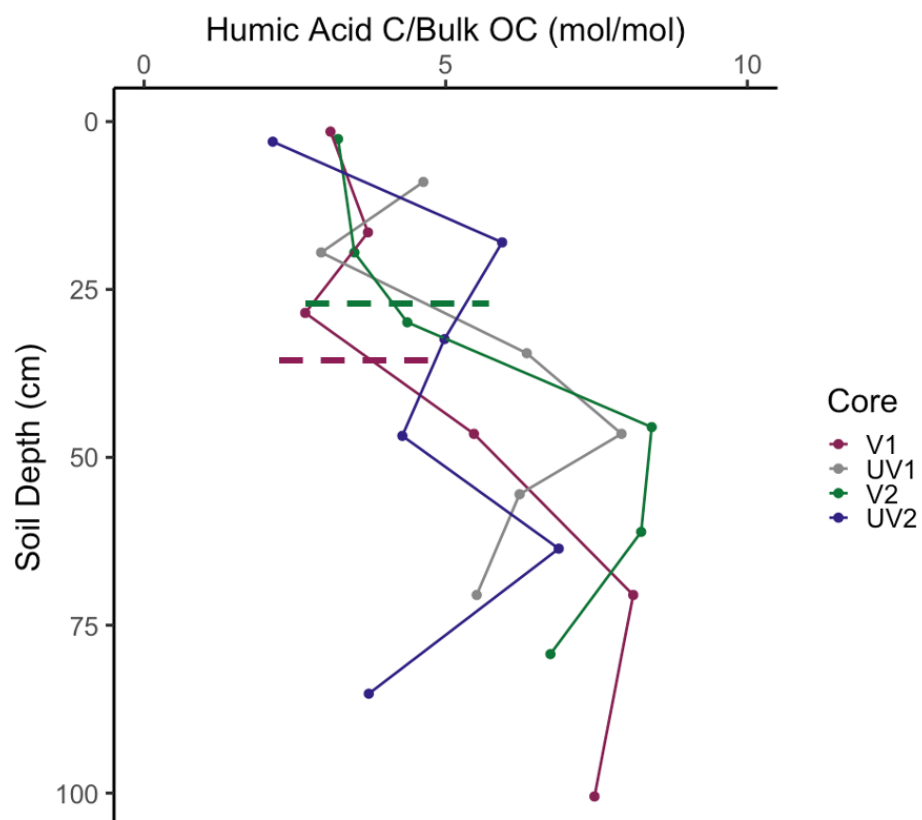


Figure A3: Humic acid C/bulk soil OC depth profile of cores taken in October 2020 and June 2021. Dashed lines indicate the bottom of the root zone in V1 (34.5 cm) and V2 (27.3 cm).

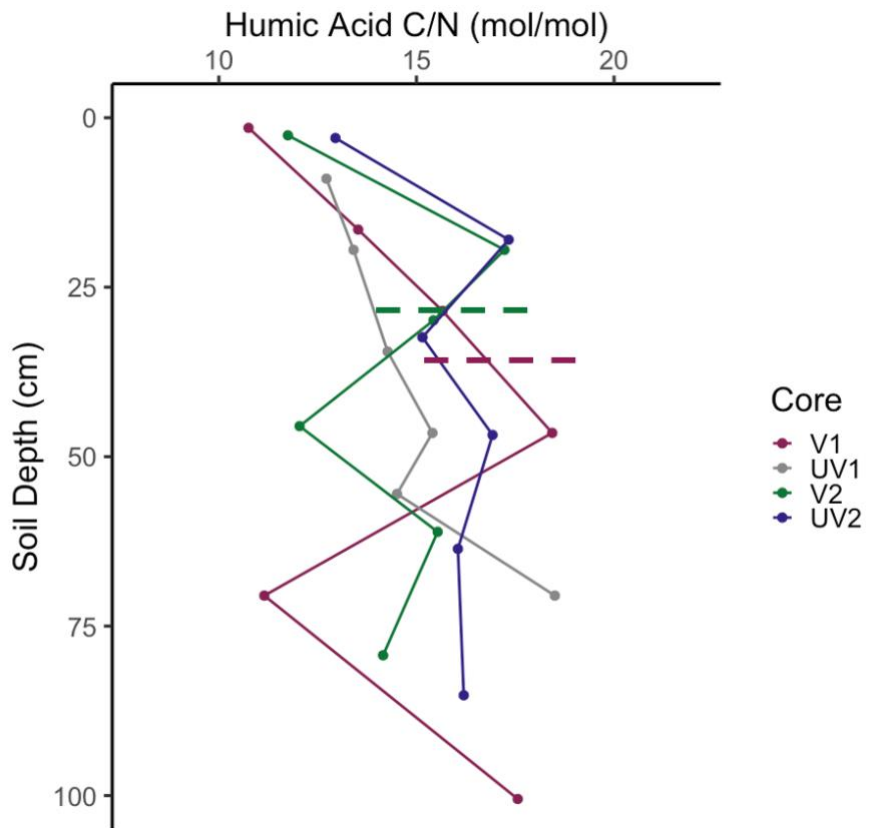


Figure A4: Humic acid C/N depth profile of cores taken in October 2020 and June 2021. Dashed lines indicate the bottom of the root zone in V1 (34.5 cm) and V2 (27.3 cm).

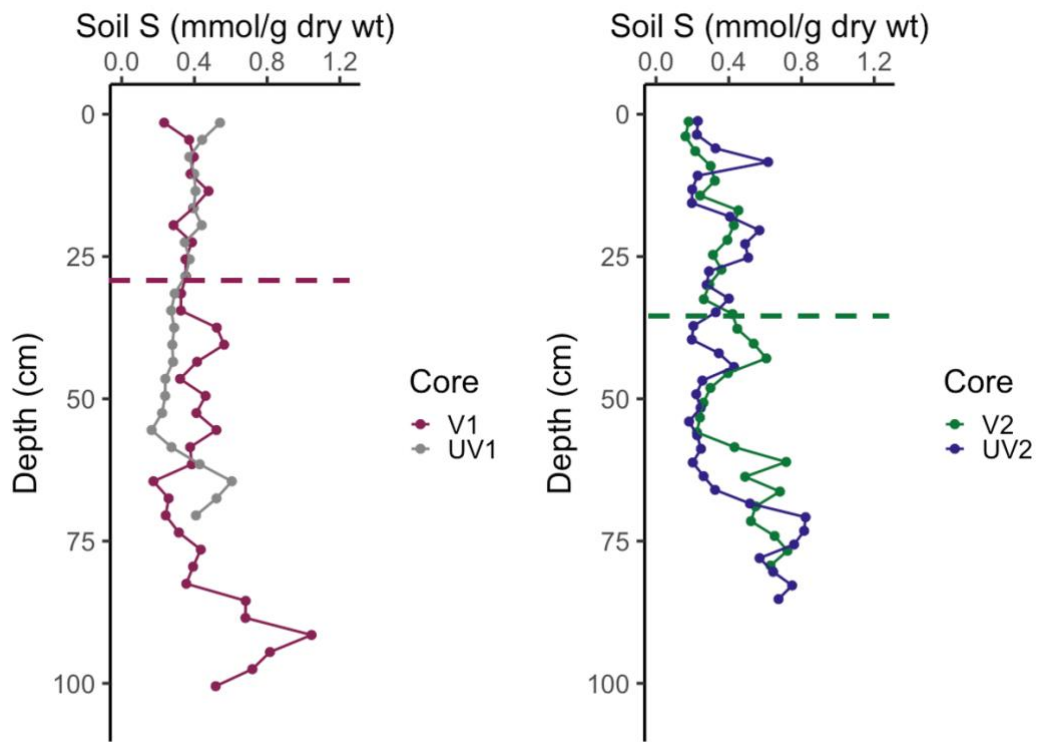


Figure A5: Soil S (organic + pyrite S) depth profiles of cores collected in October and June in vegetated and unvegetated marsh areas. Dashed lines indicate the bottom of the root zone in V1 (34.5 cm) and V2 (27.3 cm).

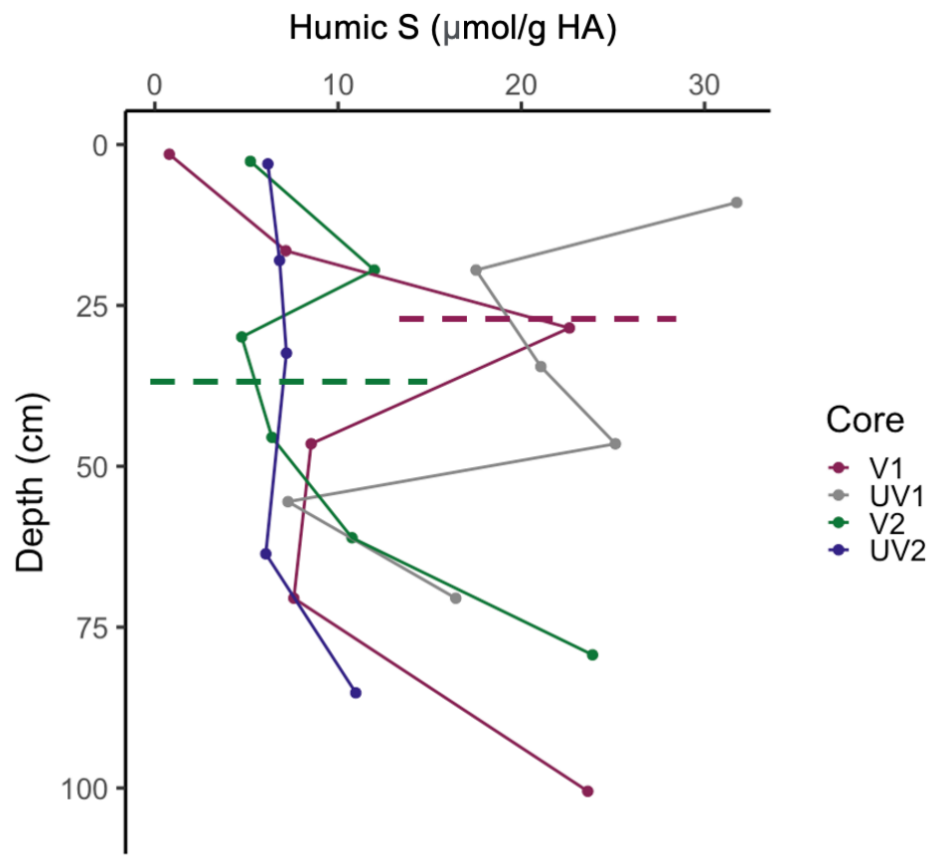


Figure A6: Humic S depth profiles of cores collected in October and June in vegetated and unvegetated marsh areas. Dashed lines indicate the bottom of the root zone in V1 (34.5 cm) and V2 (27.3 cm).

TABLES

Table A1: Depth intervals used to calculate varying accumulation rates throughout cores. Listed in terms of mass depth, OC mass depth, and length of time.

Core	Interval	Mass depth (g cm ⁻²)	OC Mass Depth (g OC cm ⁻²)	Calendar Year	Interval length (y)
V1	A	046 – 8.92	0.06 – 1.07	2020 – 1943.5	84.4
	B	9.98 – 13.67	1.13 – 1.30	1920.7 – 1863.1	57.5
V2	A	0.46 – 6.74	0.06 – 0.80	2021 – 1945.7	75.3
	B	7.65 – 10.05	0.09 – 1.05	1936.2 – 1865	71.3
UV2	A	0.05 – 1.18	0.07 – 0.38	2021– 1999.6	21.4
	B	1.69 – 4.71	0.44 – 0.64	1997.3 – 1991	6.3
	C	5.69 – 13.60	0.70 – 1.06	1986.3 – 1895.6	90.7

Table A2: Soil section depths and corresponding ^{210}Pb - and ^{137}Cs -dated soil ages.

Section ID	Uncompacted midpoint depth (cm) ¹	^{210}Pb soil age (yr)	^{210}Pb calendar year	^{137}Cs soil age (yr)	^{137}Cs calendar year
V1-1	1.5	0.0	2020.0		
V1-2	4.5	4.9	2015.1		
V1-3	7.5	9.7	2010.3		
V1-4	10.5	15.7	2004.3		
V1-5	13.5	18.0	2002.0		
V1-6	16.5	23.4	1996.6		
V1-7	19.5	30.7	1989.3		
V1-8	22.5	32.8	1987.2		
V1-9	25.5	38.2	1981.8		
V1-10	28.5	43.3	1976.7		
V1-11	31.5	50.4	1969.6		
V1-12	34.5	57.8	1962.2		
V1-13	37.5	65.3	1954.7	58	1963
V1-14	40.5	69.3	1950.7		
V1-15	43.5	76.5	1943.5		
V1-16	46.5	84.4	1935.6		
V1-17	49.5	99.3	1920.7		
V1-18	52.5	105	1915.2		
V1-19	55.5	119	1901.4		
V1-20	58.5	126	1893.5		
V1-21	61.5	157	1863.1		
UV-1	1.5	0.0	2020.0		
UV-2	4.5	5.6	2014.4		
UV-3	7.5	11.4	2008.6		
UV-4	10.5	17.4	2002.6		
UV-5	13.5	25.5	1994.5		
UV-6	16.5	33.3	1986.7		
UV-7	19.5	40.8	1979.2		
UV-8	22.5	50.2	1969.8		
UV-9	25.5	61.7	1958.3		
UV-10	28.5	69.9	1950.1		
UV-11	31.5	77.9	1942.1		
UV-12	34.5	81.5	1938.5		
UV-13	37.5	92.7	1927.3		
UV-14	40.5	113	1906.8		
UV-15	43.5	133	1886.7		

Table A2: continued.

UV-16	46.5	141	1879.3		
V2-1	1.3	0.0	2021.0		
V2-2	3.9	8.2	2012.8		
V2-3	6.5	16.7	2004.3		
V2-4	9.1	27.2	1993.8		
V2-5	11.7	30.8	1990.2		
V2-6	14.3	35.7	1985.3		
V2-7	16.9	44.5	1976.5		
V2-8	19.5	56.1	1964.9		
V2-9	22.1	63.3	1957.7		
V2-10	24.7	75.3	1945.7		
V2-11	27.3	84.8	1936.2	57	1963
V2-12	29.9	114.2	1906.8		
V2-13	32.5	156.0	1865.0		
UV2-1	1.2	0.0	2021.0		
UV2-2	3.6	3.3	2017.7		
UV2-3	6.0	7.3	2013.7		
UV2-4	8.4	15.0	2006.0		
UV2-5	10.8	21.4	1999.6		
UV2-6	13.2	23.7	1997.3		
UV2-7	15.6	25.1	1995.9		
UV2-8	18.0	26.9	1994.1		
UV2-9	20.4	28.3	1992.7		
UV2-10	22.8	30.0	1991.0		
UV2-11	25.2	34.7	1986.3	57	1963
UV2-12	27.6	45.5	1975.5		
UV2-13	30.0	52.4	1968.6		
UV2-14	32.4	60.8	1960.2		
UV2-15	34.8	76.6	1944.4		
UV2-16	37.2	93.4	1927.6		
UV2-17	39.6	125.4	1895.6		

¹The depth of cores listed here ends where ²¹⁰Pb becomes undetectable. The full length of cores is listed in Table 1.1.

Table A3: HS⁻ porewater concentrations in cores collected in October 2020 and June 2021.

Core ID	Site Conditions	Depth (cm)	HS ⁻ (μM)
V1	October vegetated	1.5	567.8
		4.5	416.3
		13.5	413.7
		16.5	432.6
		22.5	515.2
		25.5	390.1
		28.5	483.1
		31.5	584.1
		34.5	432.6
		43.5	345.9
		46.5	440.5
		52.5	373.8
		55.5	483.7
		58.5	348.0
		61.5	386.9
		64.5	382.7
		67.5	411.1
		70.5	390.6
		73.5	376.9
		76.5	386.9
79.5	443.7		
82.5	397.9		
85.5	420.0		
88.5	397.4		
91.5	372.7		
94.5	376.9		
97.5	402.7		
100.5	396.9		
UV1	October unvegetated	1.5	41.3
		4.5	136.0
		7.5	153.5
		10.5	303.8
		13.5	368.0
		16.5	382.7

Table A3: continued.

		19.5	548.3
		22.5	473.7
		25.5	752.9
		28.5	965.8
		31.5	551.0
		34.5	593.0
		37.5	1649.9
		40.5	795.5
		43.5	711.3
		46.5	859.6
		49.5	2275.1
		52.5	1561.1
		55.5	1058.9
		58.5	631.4
		61.5	1235.6
		64.5	777.1
		67.5	655.1
		70.5	692.4
V2	June vegetated	1.3	4019.6
		9.1	2748.7
		24.7	447.0
		27.3	419.7
		29.9	565.1
		32.5	514.7
		35.1	756.2
		37.7	826.0
		40.3	1994.7
		42.9	3021.7
		45.5	1821.7
		48.1	2407.8
		50.7	4171.1
		53.3	5356.6
		55.9	4760.2
		58.5	5054.8
61.1	3779.0		
63.7	3230.3		

Table A3: continued.

		66.3	2154.7
		68.9	1394.4
		71.5	1103.9
		74.1	2698.2
		76.7	1119.5
		79.3	518.9
UV2	June unvegetated	3.6	1205.8
		10.8	572.2
		13.2	289.5
		15.6	278.8
		18	321.0
		20.4	563.1
		22.8	641.0
		25.2	843.6
		27.6	804.2
		30	850.6
		32.4	978.0
		34.8	928.4
		37.2	1100.7
		39.6	3215.4
		42	3009.0
		44.4	1274.8
		46.8	1267.4
		49.2	3718.2
		51.6	3925.7
		54	1319.0
		56.4	2626.6
		58.8	1155.7
		61.2	3240.9
63.6	1109.3		
66	4601.1		
68.4	2741.6		
70.8	2187.6		
73.2	1700.7		
75.6	1568.8		
78	2718.5		

Table A3: continued.

		80.4	1619.0
		82.8	1690.2
		85.2	1279.7

Table A4: Fe²⁺ porewater concentrations in cores collected in October 2020 and June 2021.

Core ID	Site Conditions	Depth (cm)	Fe ²⁺ (μM)
V1	October vegetated	1.5	12.2
		4.5	0.0
		16.5	0.0
		22.5	0.0
UV1	October unvegetated	1.5	0.0
		4.5	1.4
		7.5	0.0
		10.5	0.2
		13.5	1.3
V2	June vegetated	1.3	502.9
		9.1	660.2
		24.7	1.1
		27.3	0.8
		29.9	0.9
		37.7	1.7
		63.7	0.8
		79.3	0.8
UV2	June unvegetated	3.6	91.9
		10.8	47.0
		13.2	0.0
		15.6	0.5
		34.8	2.5
		58.8	0.4
		82.8	4.5